PEOPLES DEMOCRATIC REPUBLIC OF ALGERIA

MINISTRY OF HIGHER EDUCATION AND SCIENTIFIC RESEARCH MOHAMED BOUDIAF UNIVERSITY MSILA

Faculty of science

Department of physics

Number:Ph/APP/03/2023

Field of material science

Branch of physics

Speciality Applied Physics

MEMORY

presented with a view to obtaining the

MASTER'S DEGREE IN PHYSICS

Speciality : Applied physics

by: **Bouhali khaled**

Studying The Physical Properties Of Indium Doped Copper Oxide Thin Films For Photocatalysis Application

BOARED OF EXAMINERS

Dr.Brri al saadi	**Professor**	**chairman**
Dr.Ibrir miloud	**Professor**	**supervisor**
Dr.meglali omar	**Professor**	**member**
Dr.mohammedi abdelkader	**Doctor**	**Assistant supervisor**

Academic year 2022-2023

Dedication

First of all, I am very grateful to Almighty God for giving me the strength and opportunity to complete this research work. I would like to express my sincere appreciation to my supervisor Prof. Dr ibrir Miloud, Department of Physics, University Mohamed Boudiaf M'sila, for his wonderful guidance and tremendous support during my master's term. Study and research. I would especially like to thank him for the generosity he has shown during this time. He is an amazing advisor who helped me through all the difficulties that I faced in my studies, research and even in my personal life. He is a great material scientist. It is a great honor for me to be his student. What I learned from him will benefit my whole life. I am very grateful to Dr. Mohammedi Abdelkader, Assistant Professor, Department of Physics, for his best wishes and support in undertaking this work. He gives me a lot of useful discussions, valuable suggestions, sharing of knowledge, trust, love and concern which helped me get through the hard times. I also thank all my teachers: Finally, I would like to express my gratitude and love from my heart to my parents and other family members my son Mohamad Yakoob and my wife for their constant support and encouragement during this research work on Bouhali Khaled Thanks!

Bouhali khaled 

Thanks

I would like to express my sincere gratitude to my thesis supervisor Professor Ibrir miloud for his advice, patience and support during my dissertation.

I would like to extend my sincere thanks and appreciation to the co-supervisor, Dr.mohammedi abdelkader, for his support and encouragement throughout this research work. I would also like to thank him for the trust he has placed in me, for his patience and calmness.

I would like to especially thank Professor Brri al saadi for his open mind, for agreeing to welcome me I am proud to have the opportunity to benefit from his extensive experience and knowledge, his far-sighted observations and suggestions.

I would like to especially thank Professor meglali omar for his open mind, for agreeing to welcome me I am proud to have the opportunity to benefit from his extensive experience and knowledge, his far-sighted observations and suggestions.

LIST OF ABBREVIATIONS

λ	Wavelength
μ	Mobility of Charge Carrier
Θ	Bragg angle
D	Crystallite size
ε	Microstrain
δ	Dislocation density
β	Full width half maximum
A	Absorbance
T	Transmittance
α	Absorption coefficient
n	Refractive index
k	Extinction coefficient
ν	Frequency
h	Planck's constant
ε_r	Real part of dielectric constant
ε_i	Imaginary part of dielectric constant
k_B	Boltzmann constant
ΔE	Activation energy
d	Thickness
σ_{opt}	Optical convection

Table of Contents

List of Figures

List of Tables

Chapter I

GENERAL INTRODUCTION

Summary

General introduction

introduction

Thin film science has emerged as a key study field in recent years. Because coatings and the synthesis of novel materials are so important in industry, there has been a great surge in novel thin film processing methods. This advancement is currently occurring in tandem with an explosion of scientific and technical advancements in microelectronics, optics, and nanotechnology [1]. A thin film is a layer of material that ranges in thickness from fractions of a nanometer (monolayer) to several micrometres. When a thin layer of solid material is created on a solid substrate, the layer thickness is said to be "thin film" if it is comparable in magnitude to the mean free path of the solid material's conduction electrons. At the moment, continuously changing requirements for thin film materials and devices are opening up new avenues for the development of novel processes, Materials and technologies. The main use of thin film science is still in microelectronics. Thin films for optical and magnetic devices, electrochemistry, protection, and electrolytes for fuel cells, ornamental coatings, and catalysis are among the emerging uses. The majority of these thin film operations are represented by a relatively recent study field known as surface engineering [2]. Thin films of metals, semiconductors, and dielectrics are becoming increasingly important for basic investigations in many sectors of science and engineering, as well as for countless practical applications. The controlled production of materials as thin films (also known as deposition) is a critical step in many applications. Thin film technology is the foundation of current technology's excellent advancement in solid state devices. Experimentation on thin films has continued in several regions of the world in order to successfully apply their qualities in scientific, technical, and industrial applications. The growing need for microelectronics and microstructural components in various fields of science and industry have significantly enlarged the field of thin film research [3, 4]. Thin film studies, which are based on the distinctive characteristics of the thickness, geometry, and structure of the film, have directly or indirectly expanded numerous new fields of inquiry in solid state physics and chemistry [5]. When compared to the bulk materials they are comprised of, thin films have several unique and interesting features. The surface qualities take precedence over the mass as the film gets thinner. The miniaturization of components such as electronic resistors, film transistors, and capacitors is also of interest. This is due to the fact that their characteristics are affected by a variety of interconnected factors as well as the deposition procedure. Thin film can be made of a single material, a composite, or a layered structure. Thin films can be both thermally stable and unstable. Thin films can be both conductive and non-conductive. Thin films are generally created by deposition, which can be done physically or chemically. Some

variables influence a film's physical, electrical, optical, and other qualities. The parameters are deposition rate, substrate temperature, environmental conditions, residual gas and pressure in the system, and material purity [6]. In recent years, oxide semiconductor thin films have become a hot issue in the world of materials research. Copper oxide CuO is a prominent oxide semiconductor because of its intriguing structural, chemical, electrical, and optical characteristics. In recent years, research on the synthesis and characterization of pure CuO and Zn, In, and Ga doped CuO has grown in popularity [7, 8]. CuO is a low energy band gap p-type semiconductor [9], and its high melting and boiling temperatures make it one of the hardest materials. It is naturally non-toxic. Because of the natural abundance of Cu, it is easily created by oxidation of copper Cu. It has several uses in electrical and optoelectronic devices. Indium In is a transition metal. The concentration of charge carriers, as well as the chemical and physical characteristics of CuO, may vary when Inis doped in CuO. Indoping in CuO thin films should result in the formation of a homogenous and stoichiometric thin film. CuO thin films may be produced using a variety of deposition processes, including electrodeposition [7, 10], chemical bath deposition [11], DC magnetron sputtering [12], vacuum evaporation [13], and spray pyrolysis technique SPT. [14]. Among these different approaches, SPT is the most basic and cost-effective [6]. SPT does not require a high-quality substrate or chemical. SPT can readily manufacture dense, porous, and multilayered films. As a result, SPT is used to deposit (In)doped CuO (CuO: In) thin films.

I.1 Applications of Thin Films

Thin films are widely employed in today's technology, and their use is projected to grow in the future. There are some current applications for thin film.

I.1.1 Optical

The following examples clearly demonstrate the use of thin films in the science of optics.

i. Resistors, condensers, and interconnects are examples of passive thin film components.
ii. Thin-film active elements (transistors, diodes)
iii. VLSI stands for Very Large Scale Integrated Circuits.
iv. Charge Coupled Device (CCD)

I.1.2 Magnetic Applications

Our application of thin films in this sector is demonstrated below.

i. Memories from audio, video, and computers
ii. Read/write magnetic heads

I.1.3 Sensor application

Our application of thin films in this sector is demonstrated below.

i. Data acquisition in aggressive environments and media Telemetry
ii. Biological Sensors

I.1.4 Biomedicine

Our application of thin films in this sector is demonstrated below.

i. Biocompatible implant coatings
ii. Cladding for depot pharmacy
iii. Neurological sensors

I.1.5 Alternative Energies

Our application of thin films in this sector is demonstrated below.

i. Solar collectors and solar cells
ii. Thermal management of architectural glasses and foils
iii. Thermal insulation (metal coated foils)

I.1.6 Cryotechnics

Our application of thin films in this sector is demonstrated below.

i. Superconducting thin films, switches, memories
ii. SQUIDS (Superconducting Quantum Interference Devices)

I.1.7 Electronics

Our application of thin films in this sector is demonstrated below.

i. Passive thin film elements (Resistors, Condensers, Interconnects)
ii. Active thin film elements (Transistors, Diodes)
iii. Integrated Circuits (VLSI, Very Large Scale Integrated Circuit)
iv. CCD (Charge Coupled Device)

I.1.8 Engineering/processing

Our application of thin films in this sector is demonstrated below.

i. Tribological Applications: Protective coatings to reduce wear corrosion and erosion, low lriction coatings.
ii. Hard coatings for cutting tools
iii. Surface passivation
iv. Protection against high temperature corrosion
v. Self-supporting coatings of refractory metals for rocket nozzles, crucibles, pipes.
vi. Decorative coatings
vii. Catalyzing coatings

I.1.9 Optoelectronics

Our application of thin films in this sector is demonstrated below.

i. Photo-detectors
ii. Image transmission
iii. Optical memories
iv. LCD/TFT
v. LED

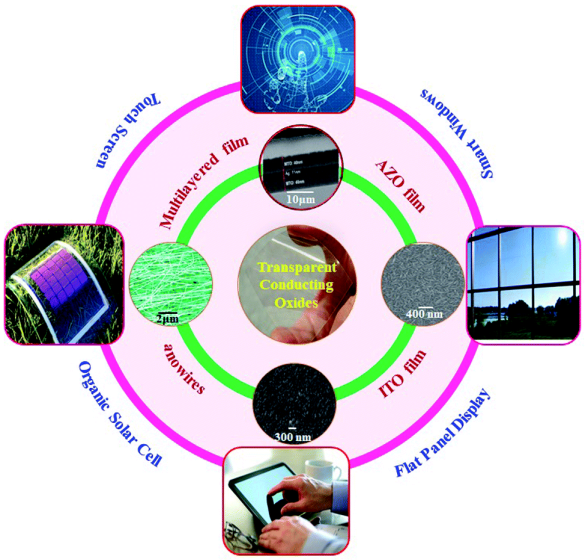

Figure I.1: Applications of Thin Films.

I.2 Oxide Semiconductors

Semiconductor is a combination of two words: Semi and Conductor. Semiconductor denotes something that can conduct electricity, but not fully. A semiconductor is a substance with conductivity midway between a conductor and an insulator. It has unusual physical qualities that place it halfway between a conductor like aluminum and an insulator like glass, figureI.2.

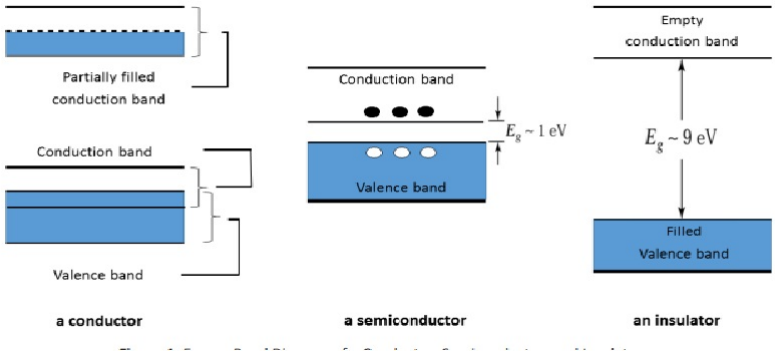

Figure I.2: Energy band diagram at absolute zero temperature for conductors, insulators and semiconductors.

Semiconductors are extremely essential because temperature and impurity concentration may readily change their conductivity. Because of its usage in computer and photovoltaic systems such as transistors, lasers, and solar cells, the quest for new semiconductor materials and the development of current materials is an important subject of research in materials science. Some semiconductor materials, such as band gap or lattice constant, can be adjustable by alloying several compounds. Materials that are transparent to the produced wavelength of light are desirable because they allow for more effective photon extraction from the bulk of the material. In other words, light generation in such transparent materials is not restricted to the surface. The refractive index is also composition-dependent and effects photon extraction efficiency from the material. Transparent electronics is one of the most advanced areas for a wide variety of device applications nowadays. The main components are wideband gap semiconductors, in which oxides of various sources play a vital role not only as a passive component but also as an active component, as seen in traditional semiconductors such as silicon. Transparent electronics has received a lot of attention in recent years and is now considered one of the most promising technologies for leading the next generation of flat panel displays due to its great electrical performance. Materials experts have identified oxide semiconductors as the next-generation semiconductor material. Copper (I) oxideCu_2O, copper (II) oxide CuO, zinc oxide ZnO, titanium dioxide TiO_2, tin dioxide SnO_2, bismuth trioxide Bi_2O_3, and other oxide semiconductors are available. They have greater transparency, a larger band gap, greater electrical conductivity, superior thermal stability, and outstanding

electrical and optical qualities. They have a wide range of applications in electronics and optoelectronics. Next-generation research will work tirelessly to establish a new sector of electronics through the advancement of oxide semiconductor device technology [15].

I.3 Photocatalysis

Photocatalysis is defined as the occurrence of a semiconductor of a metal oxide that absorbs light, leading to a chemical reaction, and this oxide is called a photocatalyst [16]. The semiconductors used in photocatalysis have the ability to absorb organic pollutants in water and oxidize them to less harmful products, such as H_2O and CO_2. We can see the photocatalytic reactions shown in Figure (1). So that the catalyst absorbs light, which leads to excitation of an electron from Valence band to conduction band and hole formation [17], the electron interacts with oxygen to form superoxide radicalsO_2 – and the hole reacts with water to form hydroxyl radicals OH[18]. These radicals are responsible for the degradation of pollutants We can apply the advanced oxidation process to numerous existing and different organic pollutants, and the process is of high importance due to its efficiency in destroying organic pollutants[16]. An advantage of photocatalysis is that it does not require expensive reagents such as hydrogen peroxide as in the case of the Fenton process

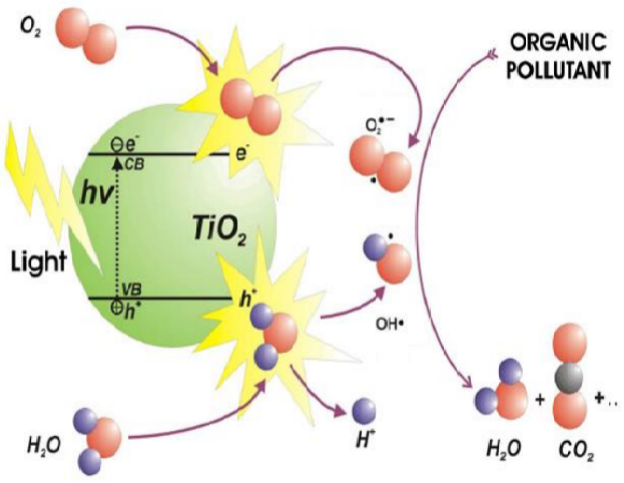

$$Cu_2O + h\nu \rightarrow Cu_2O^*(e^-_{CB} + h^+_{VB})$$

$$h^+_{VB} + H_2O \rightarrow {}^\bullet OH + H^+$$

$$O_2 + e^-_{CB} \rightarrow O_2^{\bullet -}$$

$$O_2^{\bullet -} + H^+ \rightarrow HO_2^\bullet$$

$$HO_2^\bullet + HO_2^\bullet \rightarrow H_2O_2 + O_2$$

$$O_2^{\bullet -} + HO_2^\bullet \rightarrow O_2 + HO_2^-$$

$$HO_2^- + H^+ \rightarrow H_2O_2$$

Figure I.3: Scheme explaining photocatalysis [17].

I.3.1 Catalysts for photocatalysis

The most common and used catalysts in the field of photocatalysis are TiO_2 and ZnO, due to their characteristics such as high catalytic activity, chemical stability, the most important of which is the low cost, as well as low toxicity [19] Both TiO_2 and share ZnO) in the same limitations of the catalytic property. This is because both of them have a large band gap of

about 3.1 eV, which means that they cannot absorb light in the visible range of the spectrum. TiO_2 as a catalyst has one of the best advantages, due to that It can easily photodegrade organic compounds. An example is if it is added to a basin of organically polluted water, and it is highlighted, oxidation of the organic pollutants may occur, and the water becomes clean[19]. It was found that the greater the size of the second catalyst particle The smaller the titanium oxide, the higher the catalytic reaction efficiency. One of the challenges of using both TiO_2 and ZnO[20] are

- their lack of performance in the visible spectrum
- ZnO is an n-type semiconductor, which means that Its electron concentration is greater than the hole concentration, which makes its electrical conductivity weak

I.4 Copper oxide

We can consider copper oxide CuO. It is a crucial transition metal oxide. It possesses great thermal stability as well as outstanding electrical and optical characteristics. Furthermore, it is a semiconductor material belonging to the family of transparent conductive oxides of the type (p-type) insoluble with water or bases and can be obtained from metallic copper during its transition from the metallic state to the oxide state or from Cu_2O during the phase change, according to temperature, oxidation time and others according to the following chemical reactions

$$2\,Cu + O_2 \longrightarrow 2\,CuO \tag{I.1}$$

$$2\,Cu_2O + O_2 \longrightarrow 4\,CuO \tag{I.2}$$

The following are some fundamental features of (CuO):

- ❖ Molecular Formula : CuO
- ❖ Chemical Name : Copper (II) oxide, Cupric oxide
- ❖ Molar Mass : $79.54\,g\,mol^{-1}$.
- ❖ Color : Black or brownish-black
- ❖ Appearance : Crystalline solid
- ❖ Melting Point : $1356\,^{\circ}C$.
- ❖ Boiling Point : $2000\,^{\circ}C$.
- ❖ Solubility in Water : Insoluble
- ❖ Semiconductor type : p-type
- ❖ Crystal Structure : Monocline

Copper oxide CuO is odorless, its nature is non-toxic, it is available, and its production cost is low, and it is found in nature in a dark brown color that turns black, and its optical energy gap is 1.5 eV to 3 eV, then the cutting wavelength of copper oxide is 680 nm, the absorption coefficient is estimated at 10^4 cm^{-1} at a wavelength of 500 nm it also offers a wide range of practical applications, including electrochemical cells, gas sensors, magnetic storage media, solar cells, field emitters, high-Tc superconductors, nanofluids, and catalysts [21, 22].

I.4.1 The crystal structure of copper oxide

The crystal structure of copper oxide is monoclinic, base-centred (bcc), its Space Group (c2/c)and Lattice constants(a = 4.683 Å, b = 3.4226 Å, c = 5.1288 Å, β = 99.548°) One copper oxide cell contains four molecules of (cuo) so that the Coordination of the atoms is as follows, each atom of cu or o is surrounded by four neighboring atoms of the other type (the number of nearest neighbors Z=4). For example, at Level (110)I.4, each Cu atom is surrounded by four O atoms, which are located at the corners of a parallelogram (almost a rectangle), while each O atom is surrounded by four CU atoms, which are located at the corners of a deformed tetrahedron [23].
The figureI.4 shows the constants of the crystal lattice and some other properties of copper oxide

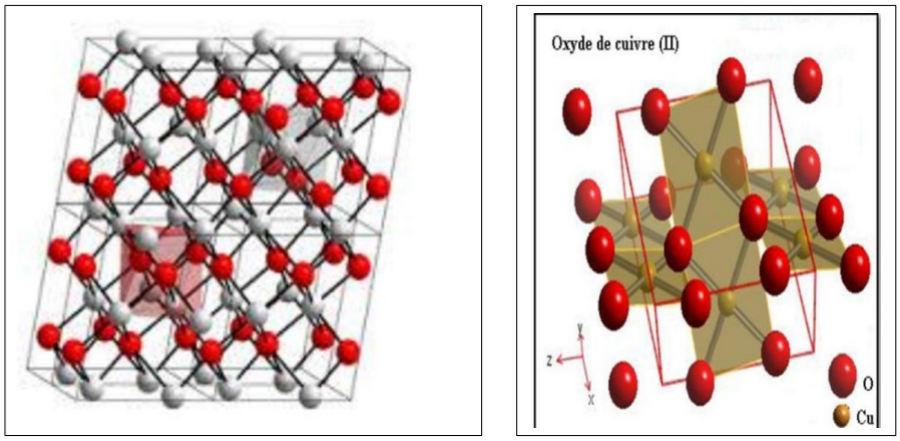

Figure I.4: The crystal structure of copper oxide.

I.5 Copper oxides for photocatalysis

The catalyst that can absorb visible light is of great importance because it allows better utilization of the sun's energy. It has been concluded that when (ZnO) and (TiO2) are used as photocatalysts, only about 3-5% of ultraviolet light is utilized[27]. This means that a large amount of energy is not used. It has been reported that the copper oxide catalyst is superior to zinc oxide and Titania in a photocatalytic reaction because it absorbs light in the visible

light region of the spectrum due to the presence of a small band gap of about (2.0-2.2) eV [20]. Copper oxide is abundant, has very low toxicity, and is cheap to prepare. [20]Copper oxide is a (p) type semiconductor, which means that its hole concentration is higher than the electron concentration. There are many parameters that affect the band gap size, electron and hole recombination rate of copper oxide, and the catalytic activity produced by the catalyst.

- Effect of size and shape on photocatalytic behavior.
- Effect of copper oxidation state on photocatalytic activity.

I.6 Indium properties

Indium atomic number 49, is a metallic element of group 13 of the periodic table. We find indium in nature isotopes: 115In (95.72 %) and 113In (4.28 %). The abundance of indium in the earth's crust is comparable to that of silver, i.e., 0.1 ppm [28]. Indium was discovered by F. REICH and T. H. RICHTER, IN A YEAR 1863 during spectral analysis for sulfur ores at the Freiberg School of Mines In Germany[29] it has been named indium after indigo Blue spectral lines led to their identification.

I.6.1 Physical Properties

Indium is a very soft silvery-white crystalline metal (softer than lead), stretchable and malleable. Indium retains its high plastic properties under cryogenic conditions temperatures. Indium can be nearly deformed indefinitely under compression, getting slightly cold-Soldered and makes a high-pitched "squeak" like tin. For folding. Indium generally increases the strength, corrosion resistance and hardness of the alloy system to which it is added. Even in small concentrations, Indium can have significant effects. The molten, indium wets the clean glass. Indium has with a low melting point 429.75 Kbut a high boiling point 2353 K. Indium becomes superconducting at3.37 K Some physical properties of indium are as follows[30, 31]

I.6.2 Chemical Properties

Metallic indium is not oxidized by air or oxygen at room temperature. It reacts directly with arsenic, antimony, the halogens, oxygen, phosphorus, sulfur, selenium, and tellurium when hotted . Indium dissolves only sluggishly in cold dilute mineral acids, but more readily in hot dilute or concentrated acids. Alkalis don't attack the massive essence. Indium forms blends with utmost other essence. Expansive solid results are formed with lead, thallium, and mercury[32]

I.7 Objectives of The Present Work

The goals of this study are to create CuO:In thin films on glass substrates using a locally constructed Spray Pyrolysis setup and to evaluate the structural, photocatalytic, and optical characteristics of the deposited thin films. (Ts) is under investigation. In addition, the influence of In concentration at optimal (Ts) of CuO:In thin films is to be examined. The following are the aims of this effort based on these research challenges:

- ✍ To synthesize CuO:In thin films with different In concentrations.
- ✍ To study the surface morphology of deposited thin films by field emission Scanning electron microscopy (FESEM), if possible.
- ✍ To estimate the elemental composition of the prepared thin films by the energy dispersive X-ray (EDX) analysis if possible.
- ✍ To analyze the structure of the deposited films by XRD analysis.
- ✍ To determine transmittance, absorbance, optical absorption coefficient, optical band gap, refractive index, dielectric constants, etc. from UV-Vis-NIR spectroscopic measurements.
- ✍ Study of the chromatography of methylene blue using ultraviolet light.
- ✍ These findings will add new knowledge in spray pyrolyzed CuO:Inthin films, which may indicate some suitable applications of these materials in the electrical and optoelectrical devices.

I.8 Outline of This Thesis

ChapterI. represents the General Introduction of this thesis.

ChapterII. focuses on the Thin Film Deposition Processes, and It is Formation.

ChapterIII. gives the Thin Film Characterization Techniques.

ChapterIV. discusses the Synthesis of Indium Doped Copper Oxide Thin Films.

ChapterV. contains the Results and Discussion of this research work.

ChapterVI. Contains the Results and Discussion of this research work.

References

[1] R. Siegel, E. Hu, and M. Roco, "Wtec panel report on r&d status and trends in nanoparticles," *Nanostructured Materials, and Nanodevices, Proceedings of the May*, pp. 8–9, 1997.

[2] J. Singh and D. E. Wolfe, "Review nano and macro-structured component fabrication by electron beam-physical vapor deposition (eb-pvd)," *Journal of materials Science*, vol. 40, pp. 1–26, 2005.

[3] A. Kumar, Y. Chung, J. Moore, and J. Smugeresky, "Surface engineering: Science and technology i. warrendale, pa: The minerals," *Metals & Materials Society*, 1999.

[4] D. A. Glocker, S. I. Shah, and C. A. Morgan, *Handbook of thin film process technology*, vol. 2. Institute of Physics Bristol, 1995.

[5] L. E. Smart and E. A. Moore, *Solid state chemistry: an introduction*. CRC press, 2012.

[6] D. Perednis and L. J. Gauckler, "Thin film deposition using spray pyrolysis," *Journal of electroceramics*, vol. 14, pp. 103–111, 2005.

[7] V. Dhanasekaran, T. Mahalingam, R. Chandramohan, J.-K. Rhee, and J. Chu, "Electrochemical deposition and characterization of cupric oxide thin films," *Thin Solid Films*, vol. 520, no. 21, pp. 6608–6613, 2012.

[8] S. Vidhya, O. Balasundaram, M. Chandramohan, *et al.*, "Influence of doping concentration on the properties of ga doped cuo thin films by the spray pyrolysis technique," *Journal of Optoelectronics and Advanced Materials*, vol. 17, no. July-August 2015, pp. 963–967, 2015.

[9] F. Marabelli, G. Parravicini, and F. Salghetti-Drioli, "Optical gap of cuo," *Physical Review B*, vol. 52, no. 3, p. 1433, 1995.

[10] N. Saadaldin, M. Alsloum, and N. Hussain, "Preparing of copper oxides thin films by chemical bath deposition (cbd) for using in environmental application," *Energy procedia*, vol. 74, pp. 1459–1465, 2015.

[11] H. Absike, Z. Essalhi, H. Labrim, B. Hartiti, N. Baaalla, M. Tahiri, B. Jaber, and H. Ez-zahraouy, "Synthesis of cuo thin films based on taguchi design for solar absorber," *Optical Materials*, vol. 118, p. 111224, 2021.

[12] G. Papadimitropoulos, N. Vourdas, V. E. Vamvakas, and D. Davazoglou, "Deposition and characterization of copper oxide thin films," in *journal of physics: conference series*, vol. 10, p. 182, IOP Publishing, 2005.

[13] H. Faiz, K. Siraj, M. Rafique, S. Naseem, and A. Anwar, "Effect of zinc induced compressive stresses on different properties of copper oxide thin films," *Indian Journal of Physics*, vol. 89, pp. 353–360, 2015.

[14] S. Roy, A. Bhuiyan, and J. Podder, "Optical and electrical properties of copper oxide thin films synthesized by spray pyrolysis technique," *Sensors & Transducers*, vol. 191, no. 8, p. 21, 2015.

[15] M. Nesa, "Characterization of zinc doped copper oxide thin films synthesized by spray pyrolysis technique," 2016.

[16] M. Umar, F. Roddick, L. Fan, and H. A. Aziz, "Application of ozone for the removal of bisphenol a from water and wastewater–a review," *Chemosphere*, vol. 90, no. 8, pp. 2197–2207, 2013.

[17] N. U. Saqib, R. Adnan, and I. Shah, "A mini-review on rare earth metal-doped tio 2 for photocatalytic remediation of wastewater," *Environmental Science and Pollution Research*, vol. 23, pp. 15941–15951, 2016.

[18] O. Monfort and G. Plesch, "Bismuth vanadate-based semiconductor photocatalysts: a short critical review on the efficiency and the mechanism of photodegradation of organic pollutants," *Environmental Science and Pollution Research*, vol. 25, pp. 19362–19379, 2018.

[19] A. Fujishima, T. N. Rao, and D. A. Tryk, "Titanium dioxide photocatalysis," *Journal of photochemistry and photobiology C: Photochemistry reviews*, vol. 1, no. 1, pp. 1–21, 2000.

[20] A. R. Makamu, *Copper oxide-carbon catalysts for the oxidation of methylene blue*. PhD thesis, Vaal University of Technology, 2020.

[21] Y. Hu, X. Zhou, Q. Han, Q. Cao, and Y. Huang, "Sensing properties of cuo–zno heterojunction gas sensors," *Materials Science and Engineering: B*, vol. 99, no. 1-3, pp. 41–43, 2003.

[22] H. Derin and K. Kantarli, "Optical characterization of thin thermal oxide films on copper by ellipsometry," *Applied Physics A*, vol. 75, pp. 391–395, 2002.

[23] M. S. Aida and Z. M. Lamri, "Cupric oxide thin films deposition for gas sensor application," 2017.

[24] A. Rahal, Elaboration des verres conducteurs par deposition de zno sur des verres ordinaires, em UNIVERSITE D ELOUED, 2013.

[25] A. Bejaoui, *Capteurs a base des couches minces d oxyde de cuivre (II)(CuO): Optimisation et mod elisation en vue de la detection de gaz.* PhD thesis, Aix-Marseille, 2013.

[26] A. Chapelle, *Élaboration et caractérisation de films minces nanocomposites obtenus par pulvérisation cathodique radiofréquence en vue de leur application dans le domaine des capteurs de CO2*. PhD thesis, Université de Toulouse, Université Toulouse III-Paul Sabatier, 2012.

[27] A. O. Ibhadon and P. Fitzpatrick, "Heterogeneous photocatalysis: recent advances and applications," *Catalysts*, vol. 3, no. 1, pp. 189–218, 2013.

[28] H. E. Suess and H. C. Urey, "Abundances of the elements," *Reviews of Modern Physics*, vol. 28, no. 1, p. 53, 1956.

[29] F. Reich and T. Richter, "Vorläufige notiz über ein neues metall," *J Prakt Chem*, vol. 89, p. 441, 1863.

[30] T. Screen, "1. fischer e., einfluss der configuration auf die wirkung der enzyme. ber. dtsch. chem. ges., 1894, 27: 2985-2993. 2. weber e., molecular recognition, in kirk-othmer encyclopedia of chemical technology, john wiley & sons, inc., 2000, online article. 3. chen b., piletsky s. & turner apf, molecular recognition: Design of" keys". comb. chem. high," *Acc. Chem. Res*, vol. 34, no. 12, pp. 938–945, 2001.

[31] J. Bailar and A. F. Trotman-Dickenson, "Comprehensive inorganic chemistry," 1973.

[32] J. D. DONALDSON, M. L. loAcniM KRDGER, E. LUDERITZ, P. WINKLER, K.-H. SCHULTE-SCHREPPINO, M. SIMON, N. FELIX, H.-r. MICKE, *et al.*, "17 secondary metals and miscellaneous alloys," *Alloys: Preparation, Properties, Applications*, p. 283, 2008.

Chapter II

Methods of deposition and formation of thin films

Summary

II.1 introduction

These days, thin films are practically everywhere and are omnipresent. To alter a material's surface or create useful gadgets, thin films are used. The choice of material heavily influences a film's qualities and, thus, its field of use. However, the properties[1] of the film can also be impacted by the nano or micrometer-scale structure of the film. Manufacturing, production, research, and applications all benefit from the thin film deposition of insulating, conducting, and dielectric materials.

II.2 Thin Film Deposition Processes

Thin film deposition is the process of putting a thin layer on a surface. Based on the nature of the deposition process, the techniques used for thin film deposition may be categorized into two major categories: physical and chemical [2]. TableII.1 the many types of deposition processes.

Physical deposition processes			Chemical deposition processes	
Evaporation	Sputtering	Other deposition processes	Gas phase	Liquid phase
Thermal	DC	Pulsed laser	Chemical vapor	Spray pyrolysis
Electron beam	RF	Cathodic arc	Thermal oxidation	Sol-gel
Laser	AC	Plasma	Chemical beam epitaxy	Dip-coating
Flash	Ion beam	Molecular beam epitaxy	Atomic layer epitaxy	Spin-coating
				Electroplating
				Anodization
				Chemical bath

Table II.1: Thin film deposition processes

Some of our most regularly used deposition of thin films processes are briefly detailed in the subsections that follow.

II.2.1 Physical deposition processes

Physical deposition methods utilize mechanical, electromechanical, or thermodynamic devices to create a thin solid layer. The material to be deposited is placed in an energetic, entropic environment, allowing particles of material to escape from its surface. A colder layer facing the source, drawing energy from the particles as they arrive and allowing them to form a solid layer. The entire system is kept in a vacuum deposition chamber to allow the particles

to flow as freely as possible. Because particles prefer to follow a straight route, films formed by physical processes are frequently directional rather than conformal.

II.2.2 Physical vapor deposition

Physical vapor deposition (PVD) is an array of methods used for creating tiny layers of material, regularly in the nanometer to micrometer range. The PVD process is depicted in FigureII.1

The PVD method is carried out in the following order:

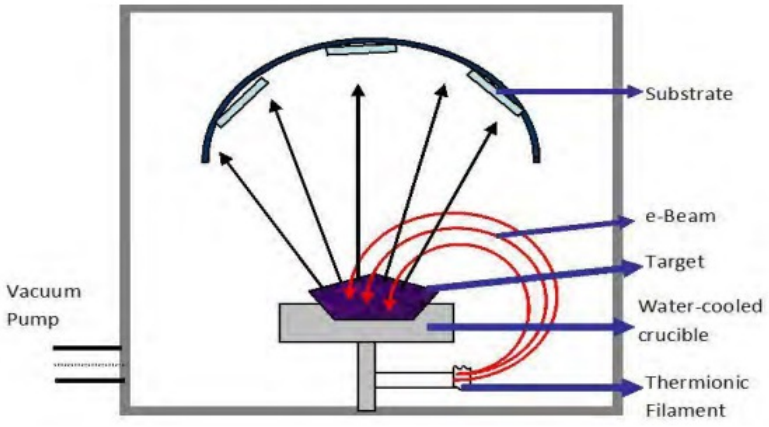

Figure II.1: Planning of the physical vapor deposition process.

1) The deposited solid substance is physically transformed to vapor.

2) The vapor phase is carried from the source to the substrate over a low-pressure zone.

3) The thin layer is formed when vapor condenses on the substrate.

II.2.3 Evaporation by heat

Thin layers are commonly produced using evaporation or sublimation processes. A huge number of materials may be evaporated, and if the evaporation is done in a vacuum system, the evaporation temperature is much lowered, as is the quantity of contaminants in the developing layer.

Although heat evaporation or vacuum evaporation is one of the oldest processes for depositing thin films, it is still frequently employed in the laboratory and in industry for depositing metals and metal alloys [3]. FigureII.2 a thermal evaporation system schematic. The substance to be deposited is placed in a crucible, which is a heated container. A significant current is used to

restively heat the crucible. In the material in the crucible heats up, it emits a vapor whose atoms move in straight lines until they hit a surface and collect in a film.

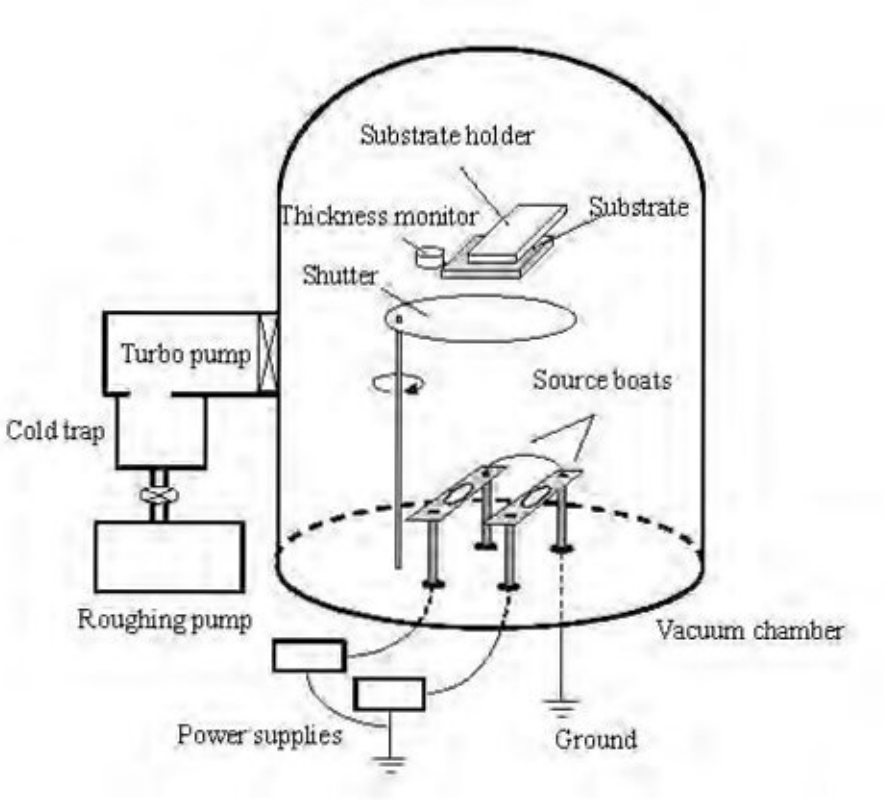

Figure II.2: Thermal evaporation system schematic diagram..

II.2.4 Sputtering

When a target material's surface is attacked with energetic particles, the surface atom can be ejected: this is known as sputtering. The atoms discharged can be condensed on a substrate to produce a thin film. This approach offers several benefits over traditional evaporation procedures, including the absence of container contamination.
It is also feasible to deposit alloy films that maintain the original target material's composition. Figure II.3 depicts a sputtering system diagram. The earliest forms of sputtering include direct current (DC) sputtering, radio frequency (RF) sputtering, and magnetron sputtering [4]. The two novel technologies for deposition of thin films for use in superconducting and magnetic films are high pressure oxygen sputtering and facing target sputtering.

II.2.5 Pulsed laser deposition

PLD (pulsed laser deposition) is an enhanced thermal technique for depositing alloys or compounds with a defined chemical composition. A high-power pulsed laser $(1J/shot)$ is shone onto the target or source materials via a quartz window for laser deposition. To improve

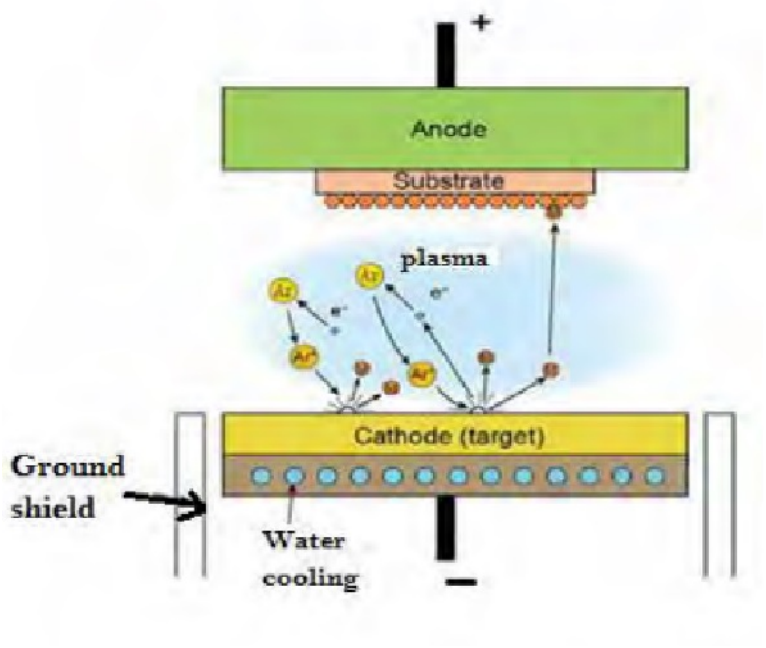

Figure II.3: A sputtering system diagram.

the energy density of the laser power on the target source, a quartz lens is utilized. Abraded or evaporated surface atoms are gathered on surrounding substrate surfaces to create thin films [5].

In a vacuum, the target material is locally heated to the melting point, melted, and evaporated. The laser pulse may also supply photo-emitted electrons from the target to form a plasma plume, and the evaporation mechanism may be complicated due to the fact that the process comprises both the thermal and plasma processes. One can achieve the required deposition rate and structure quality by adjusting several factors such as ablation energy, base vacuum level, background oxygen pressure, distance between target and substrate, and substrate temperature. Figure 2.4 II.4 depicts a PLD system diagram.

II.3 Chemical deposition processes

A fluid precursor undergoes a chemical transformation at a solid surface, forming a solid layer. Chemical deposition technologies are broadly categorized into two types: gas phase techniques and liquid or solution phase techniques.

II.3.1 Chemical vapor deposition

Chemical vapor deposition (CVD) is a material production process in which vapor phase elements react to generate a solid coating at a surface [6]. Because the chemical reaction is a crucial feature of this approach, it must be thoroughly understood in addition to the regulation

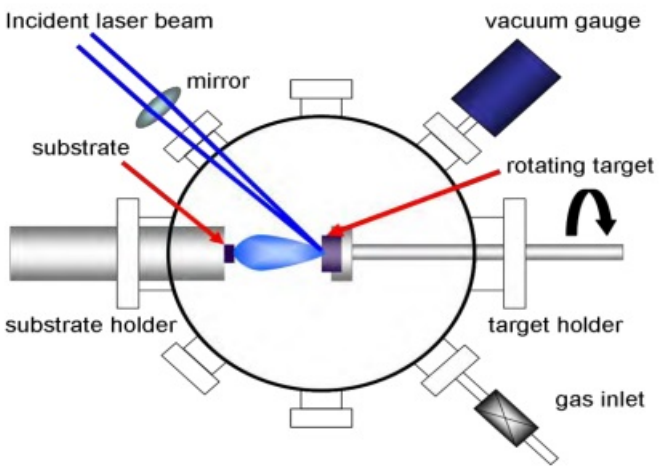

Figure II.4: A schematic of a pulsed laser deposition system.

of the conventional deposition process factors.
Pyrolysis, reduction, oxidation, hydrolysis, synthetic chemical transport reaction, and other chemical processes are used in CVD to create solids. It has emerged as one of the most potent thin-film growth methods. One of the reasons for the increasing use of CVD technologies is the ability to make a wide range of crystalline and amorphous films and coatings of metals, semiconductors, and compounds with high purity and desired characteristics. Furthermore, the ability to controllably create films with significantly changing stoichiometry distinguishes CVD from other deposition processes.
Additional advantages include minimal equipment and operating costs, appropriateness for batch and semi-continuous operation, and compatibility with other processes. Figure II.5 is a CVD process schematic.
Vapor Phase Epitaxy (VPE) is used when CVD is used to deposit single crystal films, Metal-organic CVD (MOCVD) is used when the precursor gas is a metal-organic species, Plasma Enhanced CVD (PECVD) is used to induce or enhance decomposition and reaction, and Low Pressure CVD (LPCVD) is used when the pressure is less than ambient.

II.3.2 Deposition through a chemical bath

Chemical bath deposition (CBD), also known as chemical solution deposition (CSD) or chemical deposition (CD), is perhaps the simplest technology available for this purpose.
It is not a novel technology; in 1835, Lie big published the first silver deposition, the silver mirror deposition utilizing a chemical solution process. The process of deposition was originally described in 1869. All that is needed for these processes is a vessel to hold the solution (often an aqueous solution of common chemicals) and the substrate to be redeposited on. Additionally, a mechanism for stirring and a thermal stated bath to maintain a specified

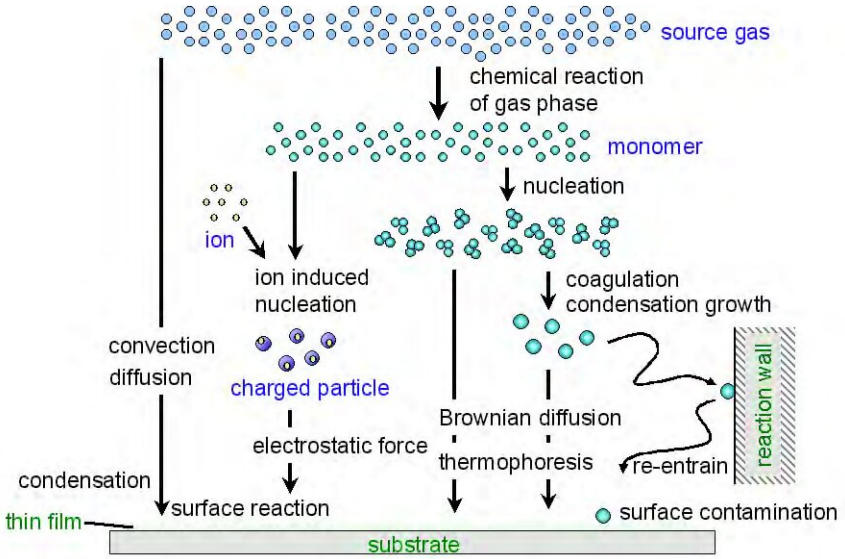

Figure II.5: Schematic diagram of a CVD process.

and consistent temperature are possibilities that may be useful [7, 8].

CBD is a technique for producing thin films of certain materials on a substrate bathed in an aqueous bath containing suitable chemicals at temperatures ranging from ambient temperature to 100 degrees Celsius.

Figure II.6 is a CBD process diagram. CBD is generated in two stages: nucleation and particle development. It also includes the controlled precipitation of a chemical from solution on a suitable substrate. The process has several benefits over more established vapor phase synthetic techniques for semiconductor materials, such as CVD and MBE, among others.

Varying the solution pH, temperature, and reagent concentration aides issues such as control of film thickness and deposition rate, as well as CBD's capacity to cover vast areas in a repeatable and low-cost method. For CBD growth, two techniques are commonly used: single dip, in which the substrate is submerged in the reaction just once, and multiple dips, in which the same substrate is coated repeatedly to generate a thicker film.

II.3.3 The Sol-Gel method

The sol-gel method was created in the 1960s as a reaction to the nuclear industry's demand for novel synthesis methods.

A technique with less dust (relative to the ceramic approach) and a lower sintering temperature was required. Furthermore, the synthesis should be controllable through remote. The sol-gel technique is a wet chemical method for producing colloidal dispersion of oxides that may be converted into powders, fibers, thin films, and monoliths [9].

The sol-gel process, in general, consists of hydrolysis and condensation reactions. Sol-gel coating is a method of producing a single or multi-component oxide coating that can be glass,

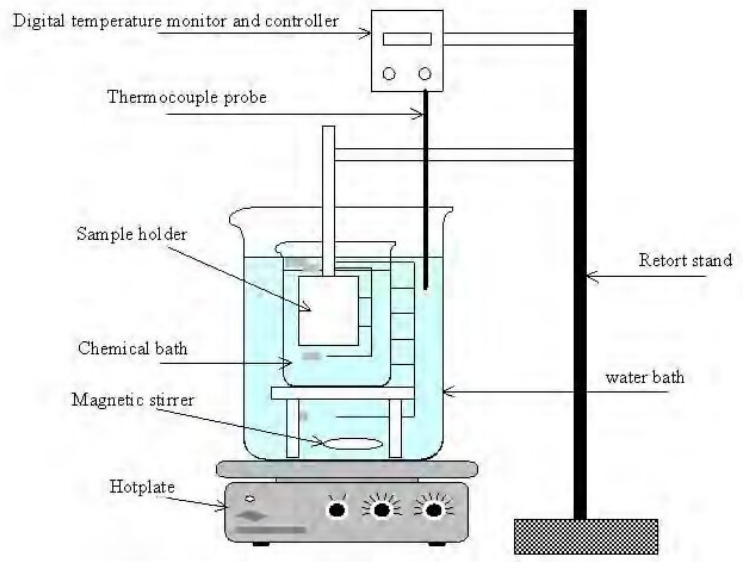

Figure II.6: A CBD system schematic.

glass ceramic, or crystalline ceramic depending on the procedure. Furthermore, nanomaterials employed in current ceramic and device technologies necessitate high purity and allow for greater control over composition and structure. Figure II.7 is a sol-gel method diagram.
One of the intriguing ways is the sol-gel method, which offers several benefits [10].
The following are some examples:

- The chemical reactants used in the sol-gel process may be easily refined using distillation and crystallization.

- All strong components are molecularly combined in the solution, resulting in a high degree of film uniformity.

- Organic or inorganic salts can be added to adjust he microstructure or to improve the structural, optical and electrical properties of oxide films.

- The sol-gel process is almost solely used to create translucent layers with great planarian and surface quality.

II.3.4 Spray pyrolysis method

Spray pyrolysis technique (SPT) is a method of creating thin films by spraying a solution over a heated surface, where the ingredients react to generate a chemical molecule [11].
The chemical reactants are chosen in such a way that the products other than the intended molecule are volatile at the deposition temperature. Spray pyrolysis, in contrast to many

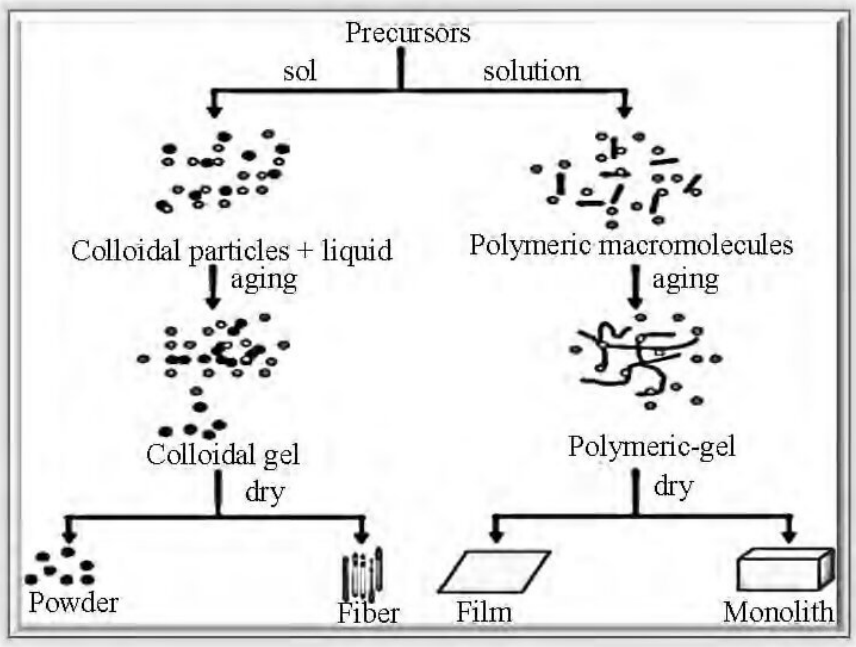

Figure II.7: Sol-gel method generalized scheme.

other film deposition procedures, is a fairly simple and very low-cost processing approach, particularly in terms of equipment expenses. It provides an exceedingly simple method for preparing films of any composition.

SPT does not necessitate the use of high-quality substrates or chemicals. The process has been used for dense film deposition, porous film deposition, and powder manufacturing. This adaptable approach may also be used to create multi-layered films [12].

Following that, the simplicity of the equipment and the high productivity of this process on a wide scale made it a very appealing method for the creation of thin films of noble metals, metal oxides, spinel oxides, calcogenides, and superconducting compounds. The quality and qualities of thin films in the SPT process are heavily influenced by the preparation conditions. Recently, there has been a focus on two aspects: (1) atomization methods to more precisely regulate droplet size and distribution, and (2) the use of beginning chemicals such as organic to generate highly oriented thin films, which appears to be more promising.

Chemical spray deposition techniques were categorized by Viguie and Spitz based on the kind of reaction. In process A, the droplet remains on the surface while the solvent evaporates, leaving behind a solid that may react further in the dry state.

The solvent evaporates before the droplet reaches the surface in process B, and the dry solid impinges on the surface, where breakdown begins. As the droplet reaches the substrate, the solvent vaporizes; the solid then melts and vaporizes, and the vapor diffuses to the substrate, where it undergoes a heterogeneous reaction. The complete reaction occurs in the vapor state in procedure D. The ambient temperature, carrier gas flow rate, nozzle-to-substrate distance, droplet radius, solution concentration, solution flow rate, and - for continuous processes -

substrate motion are all critical factors in all operations. The majority of spray pyrolysis depositions are of type A or B. Figure II.8 depicts a flow chart for a block diagram comprising several SPT stages.

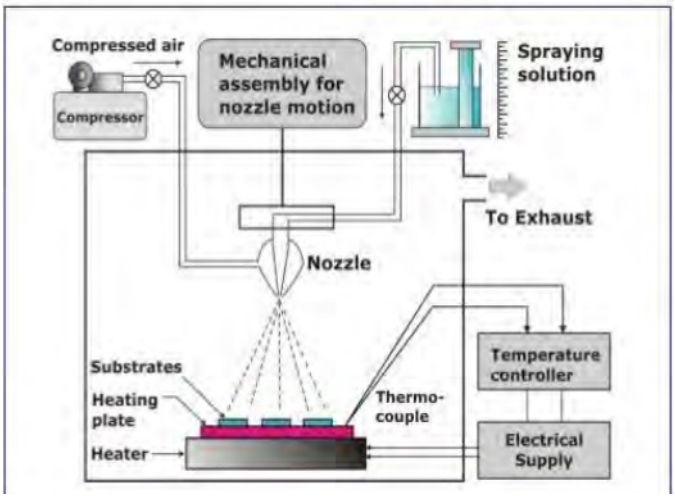

Figure II.8: SPT diagram of several steps.

II.3.5 Spin coating

Spin coating is a method of applying homogeneous, thin coatings on flat surfaces. A common procedure consists of placing a tiny puddle of a fluid resin into the center of a substrate and then rotating the substrate at high speed (usually about 3000 rpm) (Mitzi et al. 2004). The resin will spread to and finally over the edge of the substrate due to centrifugal force, leaving a thin layer of resin on the surface. The final film thickness and other attributes will be determined by the nature of the resin (viscosity, drying rate, solids, surface tension, and so on) as well as the spin parameters. Figure 2.9: Spin coating procedure diagram

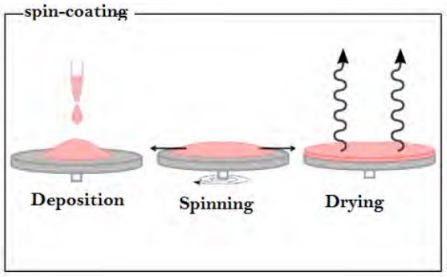

Figure II.9: : A diagram of spin coating technique.

process. A spin coating, or simply spinner, is a spin coating machine. The fluid is spun off the edges of the substrate while the rotation continues until the appropriate thickness of the film is reached. The used solvent is generally volatile and evaporates at the same time. As a result, the thinner the coating, the faster the angular speed of spinning. The concentration of

the solution and the solvent also influence the thickness of the film (Hellstrom 2007). Spin coating is commonly used in microfabrication to make thin films with thicknesses as low as 10 nm.

II.4 Formation of Thin Films

Individual atoms are deposited on a substrate to form thin films. A sufficient time gap must exist between the two subsequent depositions of atoms and layers in order for these to occupy the lowest potential energy configuration. A typical thin-film deposition method consists of three key phases [13]:

+ Creation of the necessary atomic, molecular, or ionic species

+ Transfer of these organisms through a medium to the substrate

+ Condensation on the substrate to produce a solid deposit, either directly or by a chemical and/or electrochemical process.

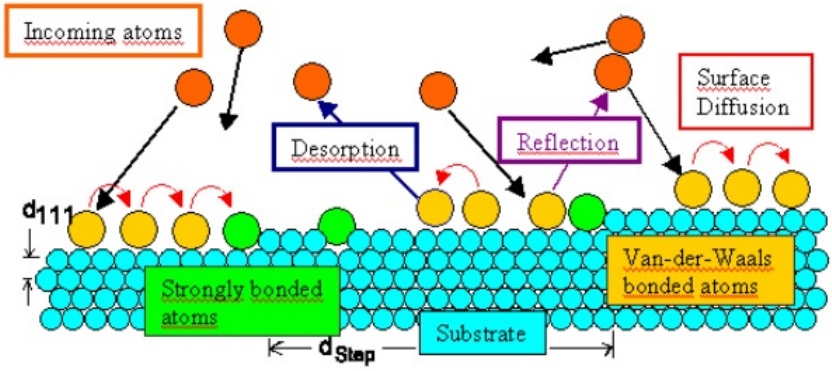

Figure II.10: Schematic diagram of thin film formation process

II.4.1 Different stages of film formation

There are three distinct methods of thin film condensation based on the intensity of contact between the atoms of the expanding film and the atoms of the film and substrate. These are the.

1) Layer-by-layer growth (Frank-van der Merwe mechanism): Because the adsorbate substrate contact predominates over the adsorbate-adsorbate interaction, a new layer begins to form only after the preceding layer has been finished.
2) Island formation (Vollmer-Weber mechanism): Adsorbate-adsorbate interaction dominates, resulting in multilayer island formation.

3) Layer-plus-island growth (Dranski-Krastanov mechanism): It is a particular interesting case that has recently been exploited in the production of nanometre scale islands. After the formation of one or more compete monolayers, three-dimensional islands nucleate and grow on top of the complete layer.

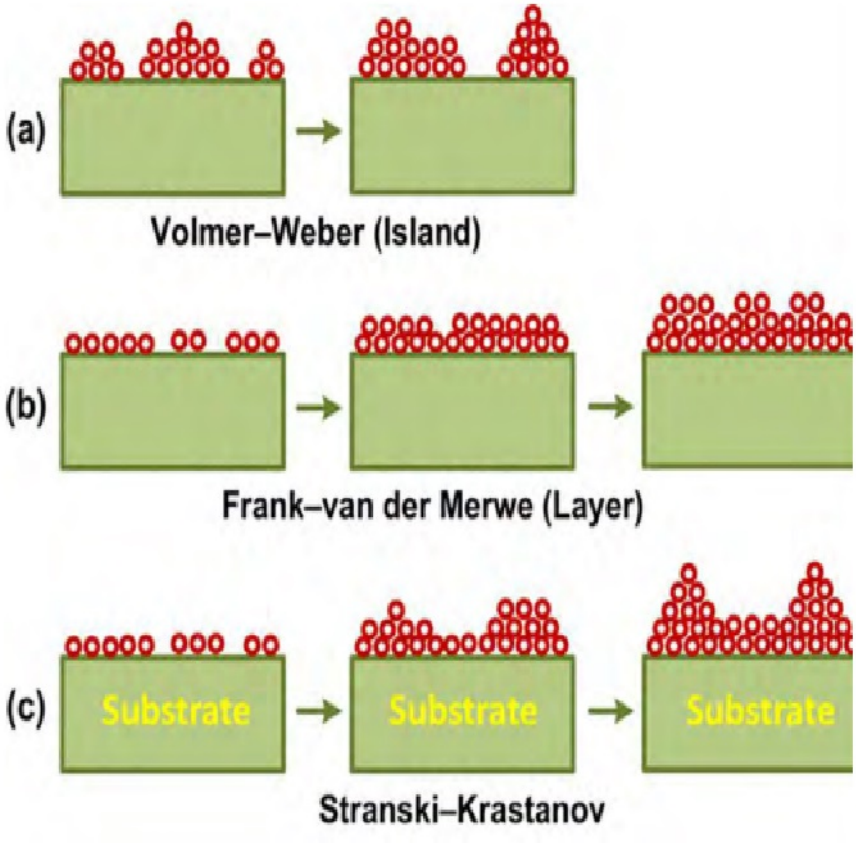

Figure II.11: Layer-by-layer mode II) Island growth mode and III) Layer-plus-island growth mode..

In most situations, mechanism II occurs and is briefly addressed.

II.4.1.1 Condensation

Condensation is simply the conversion of a gas into a liquid or solid. The sole prerequisite for condensation to occur from a thermodynamic standpoint is that the partial pressure of the film material in the gas phase is equal to or greater than its vapor pressure. At such temperature, the partial pressure of the film material in the gas phase is equal to or greater than its vapor pressure in the condensed phase. At that temperature, it is in the condensed phase. The interaction of a vapor atom with the affected surface determines its condensation. The impacting atom is drawn to the surface by the atoms' instantaneous dipole and quadruple moments. On the surface, there are atoms. As a result, the atom's velocity component normal

to the surface is lost. In a short period of time, provided that the incident kinetic energy is not excessive. The atom of vapor is. Physically absorbed (referred to as an atom), yet it may or may not be totally thermally balanced [14]. Because of the heat activation of the surface and its own kinetic energy, it can travel over the surface by leaping from one potential well to another. Because of the thermal activation of the surface and its own kinetic energy parallel to the surface, it can travel from one potential well to the other. The adatom has a limited duration on the surface. It can connect with other adatoms during this period to create a stable group and be chemically absorbed, releasing energy. Chemically absorbed with the emission of condensation heat. Adatoms re-evaporate or desorb into the vapour phase if they are not absorbed. As a result, condensation is the end result of As a result, condensation is the net outcome of the adsorption and desorption processes being balanced. The "condensation coefficient" or "adhesion coefficient" is the likelihood of an impacting atom being integrated into the substrate (surface). It is determined by the ratio of The "condensation coefficient" or "adhesion coefficient" is the likelihood of an impacting atom being integrated into the substrate (surface). In fact, the coefficient of adhesion is sometimes so low that it is not detectable using standard procedures. On the other hand, the bonding coefficient is greatly reliant on the overall duration the substrate was subjected to the impact, as well as the temperature of the substrate. The substrate's temperature. The re-evaporation of monomers from portions of the substrate beyond the capture zones surrounding each stable core is commonly used to explain a non-unitary bond coefficient. Each stable core has capture zones [15].

II.4.1.2 Nucleation

Condensation begins with the production of a tiny group from the interaction of many adsorbed atoms. Multiple adsorbed atoms. These groupings are known as nuclei, and the process by which they originate is known as nucleation. Nucleation is the process of generating clusters. During film formation, two types of nucleation occur: (i) homogeneous nucleation and (ii) heterogeneous nucleation.

1) **Homogeneous nucleation**
   In the creation of a collection of atoms, the total free energy is utilized [16].

2) **Heterogeneous nucleation**
   Specific cluster morphologies are generated by atoms colliding on the surface of the substrate, and its saturation is sufficiently high in the vapour phase [17]. They expand at first by increasing free energy until they reach a certain size, after which they continue to grow by decreasing free energy. Free energy. When the substrate temperature is low or the saturation in super saturations is very high, the crucial nucleus may be a single atom that will couple with another atom by chance to form an atom of the same size,

according to atomistic theory. By coincidence with another atom to form a stable group and develop spontaneously.

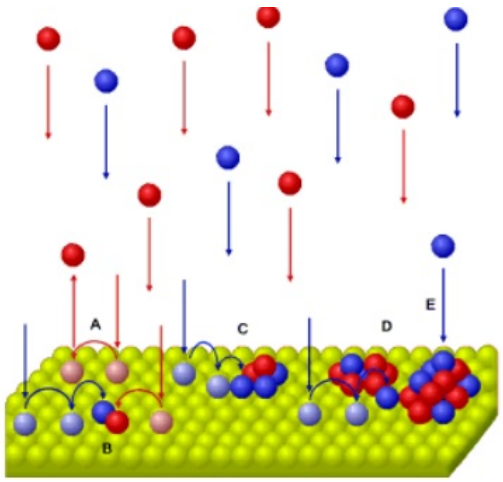

Figure II.12: Adatom processes (sort red and blue) during heterogeneous condensation.

II.4.1.3 Growth

The ultimate and completed stage in the development of a thin film is growth. There are several stages. From the earliest nucleation of deposits to the final condition of producing a continuous three-dimensional film during the growth process. Film that is both continuous and three-dimensional. Many researchers have noticed these stages of film development through electron microscope experiments and other studies. They have They apply not only to deposits condensing from the vapor phase, but also to solutions, electroplating, chemical deposition, and so on. They apply not only to deposits condensing from the vapor phase, but also to solution deposits, electrodeposition, chemical reactions, anoxic oxidation, and so on. Although. Although the control parameters may fluctuate somewhat or significantly from case to case, these processes have been explicitly defined [18, 19].

1) **Nucleation and Island Formation**

   When an electron microscope is used to examine a substrate hit by condensed monomers, the first sign of condensation is a quick burst of condensed monomer nuclei. When an electron microscope is used to examine a substrate subjected to condensed monomer impact, the first sign of condensation is a quick burst of nuclei of rather uniform size. Size is generally consistent. The nuclei expand in three dimensions, although growth parallel to the substrate is more critical than normal growth. The parallel development of the nuclei to the substrate is more critical than normal growth. This is most likely because growth happens. This is most likely owing to the fact that development proceeds by surface diffusion of monomers onto the substrate rather than direct effect of the vapor phase. The vapor phase has a direct influence. The proclivity to build an island configuration is high.

i. high substrate temperature
ii. low boiling point of film material
iii. low deposition rate
iv. weak binding energy between film material and substrate
v. high surface energy of the film material and
vi. low surface energy of the substrate

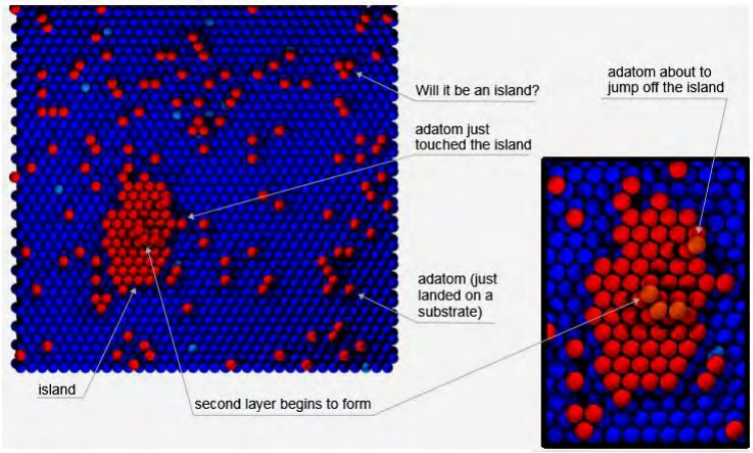

Figure II.13: The mechanism of formation of island stage during thin film growth

2) **The coalescence stage**

The coalescence phase follows the film production process, in which the tiny islands begin to merge with each other in an attempt to shrink the substrate. The substrate's surface area. This propensity to create bigger islands is known as agglomeration, and it is aided by the adsorbed species' greater surface mobility. This propensity to create bigger islands is known as agglomeration, and it is aided by increasing the surface mobility of adsorbed species, such as by raising the substrate temperature. It is possible for new nuclei to arise in some instances.

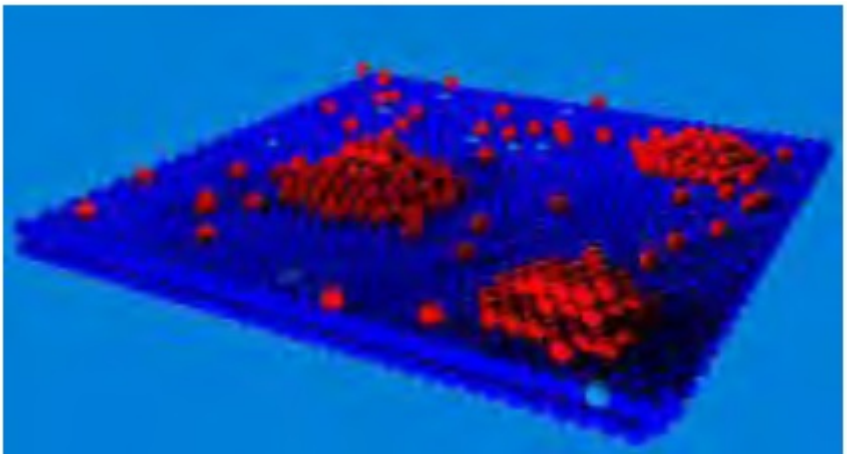

Figure II.14: Schematic diagram of coalescence stage.

As a result of coalescence, on newly exposed regions. As the islands grow in size due to fresh deposition and migrate closer together, the larger ones appear to develop as a result of the coalescence of the smaller ones. Furthermore, before coalescence, nuclei with well-defined crystallographic forms become rounded [20]. The island is If the composite island is allowed long enough to interact with its neighbors, it will revert to crystallographic form.

3) **channel stage**

As bigger islands develop together, they form a network structure on the substrate with pathways of linked holes of exposed substrate. Secondary nucleation develops in these channels as deposition proceeds, becoming the last step of nucleation.

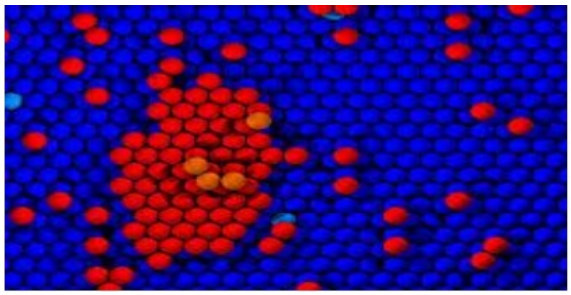

Figure II.15: Schematic diagram of channel stage

em **The continuous film stage**

The final step of film development is the continuous film stage. It is a laborious procedure that takes a significant number of deposits to fill the empty channels. Coalescence releases vast regions at the channel stage. Secondary deposits fill these vacant passageways. Secondary nucleation, growth, and coalescence fill these vacant channels,

resulting in the formation of a continuous film. Figure II.16 depicts the various stages of film development schematically.

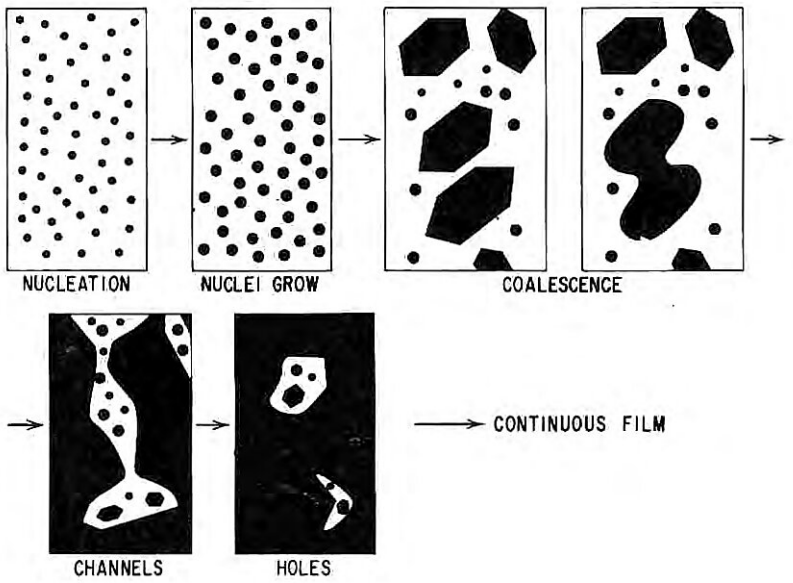

Figure II.16: Different stages of thin film growth. growth mode.

References

[1] M. Ohring *et al.*, "Mechanical properties of thin films," *Materials Science of Thin Films*, pp. 711–781, 2002.

[2] K. Chopra, "Thin film phenomena mc graw hill co," *New York, USA*, 1969.

[3] L. I. Maissel and R. Glang, "Handbook of thin film technology mcgraw-hill," *New York*, pp. p12–21, 1970.

[4] R. Behrisch *et al.*, *Sputtering by particle bombardment*, vol. 1. Springer-Verlag New York, 1981.

[5] M. J. Aziz, "Film growth mechanisms in pulsed laser deposition," *Applied Physics A*, vol. 93, pp. 579–587, 2008.

[6] D. Dobkin and M. K. Zuraw, *Principles of chemical vapor deposition*. Springer Science & Business Media, 2003.

[7] K. Chopra, "R, c. kainthla, dk pandya and ap thakoor," *Physics of Thin Films*, vol. 12, p. 168, 1982.

[8] C. Lokhande, "A chemical method for preparation of metal sulfide thin films," *Materials chemistry and physics*, vol. 28, no. 1, pp. 145–149, 1991.

[9] L. L. Hench and J. K. West, "The sol-gel process," *Chemical reviews*, vol. 90, no. 1, pp. 33–72, 1990.

[10] S. ILICAN, M. Çağlar, and Y. Çağlar, "The effect of deposition parameters on the physical properties of cd xzn1-xs films deposited by spray pyrolysis method," *journal of optoelectronics and advanced materials*, vol. 9, no. 5, 2007.

[11] R. Chamberlin and J. Skarman, "Chemical spray deposition process for inorganic films," *Journal of the Electrochemical Society*, vol. 113, no. 1, p. 86, 1966.

[12] D. Perednis and L. J. Gauckler, "Thin film deposition using spray pyrolysis," *Journal of electroceramics*, vol. 14, pp. 103–111, 2005.

[13] H. Hartnagel, *Semiconducting transparent thin films*. CRC Press, 1995.

[14] Z. Zhang and M. G. Lagally, "Atomistic processes in the early stages of thin-film growth," *Science*, vol. 276, no. 5311, pp. 377–383, 1997.

[15] K. Chopra, "Nucleation, growth and structure of films," *Thin Film Phenomena, McGraw-Hill, New York*, p. 137, 1969.

[16] M. R. Waugh, *The synthesis, characterisation and application of transparent conducting thin films*. PhD thesis, UCL (University College London), 2011.

[17] X. Zhang and E. Jiang, "The nucleation and initial growth of iron films deposited by facing targets sputtering," *Journal of magnetism and magnetic materials*, vol. 121, no. 1-3, pp. 46–48, 1993.

[18] X.-L. Guo, H. Tabata, and T. Kawai, "Pulsed laser reactive deposition of p-type zno film enhanced by an electron cyclotron resonance source," *Journal of Crystal Growth*, vol. 223, no. 1-2, pp. 135–139, 2001.

[19] P. Jensen, A.-L. Barabási, H. Larralde, S. Havlin, and H. EUGENE STANLEY, "A fractal model for the first stages of thin film growth," *fractals*, vol. 4, no. 03, pp. 321–329, 1996.

[20] C. Ratsch and J. Venables, "Nucleation theory and the early stages of thin film growth," *Journal of Vacuum Science & Technology A: Vacuum, Surfaces, and Films*, vol. 21, no. 5, pp. S96–S109, 2003.

Chapter III

TECHNIQUES FOR CHARACTERIZING THIN FILMS

Summary

TECHNIQUES FOR CHARACTERIZING THIN FILMS

The structural, surface morphological, electrical, and optical characteristics of CuO and CuO:Zn thin films are studied. Properties of morphology, electricity, and optics. X-ray diffraction (XRD) is used to research structure, SEM is used to analyze nature, and (FESEM) is used to determine surface shape and energy dispersive Surface morphology is identified using X-ray spectroscopy (EDX). The composition of the produced films is studied using energy dispersive X-ray spectroscopy (EDX). The optical properties The optical characteristics were determined using a UV-Visible spectrophotometer and transmittance and absorbance spectra. The electrical resistivity of the films is measured using the four-point probe method. The concept, function, and significance of This chapter briefly describes the concept, operation, and significance of each technique, as well as the accompanying theory.

III.1 Characterization of Structure

Science and engineering are founded on the formation of thin films and super lattices, as well as the formation of patterns on a sub-micrometer scale. To comprehend their structural qualities, A thorough structural characterization is necessary to comprehend the structural characteristics of these nanostructures. XRD TECHNIQUES allow us to investigate the internal structure of layers as well as the quality of interfaces between various materials in a multilayer construction. The interface quality of different materials in a multilayer. The most conclusive structural information is provided by XRD.

III.1.1 Diffraction of X-rays

Scientists were able to examine crystal structure at the atomic level with the discovery of X-rays in 1895. On an atomic scale. XRD has been employed in two key areas: characterization of the fingerprint of crystalline materials and structural determination [1]. Each and every crystalline solid Each crystalline solid has a distinct X-ray powder pattern that may be used as a "fingerprint" to identify it. "Fingerprint" is used to identify it. Once the substance has been identified, X-ray crystallography may be performed. X-ray crystallography may be used to identify its structure, or how the atoms fit together and what they are doing in the crystalline form. The inter-atomic distance and angle in the crystalline state, etc.
The XRD technique is the most straightforward way to determine the size and shape of a compound's unit cell. XRD is the most effective method for determining the size and shape of a compound's unit cell. X-rays are electromagnetic waves with a wavelength of around 1. When X-rays strike a crystal surface, they are reflected by the surface.

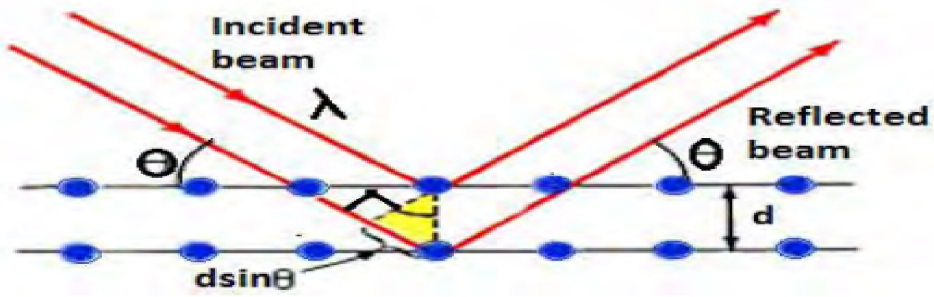

Figure III.1: X-ray reflection from two planes of atoms in a solid.

The reflection follows Bragg's law as follows:

$$2dsin\theta = n\lambda \tag{III.1}$$

Where (d) is the distance between crystal planes, (θ) is the X-ray incidence angle, (λ) is the X-ray wavelength, and (n) is a positive integer. According to Bragg's rule, diffraction is only feasible when ($\lambda < 2$d).

It is feasible to determine the average grain size of the thin film [2] from the width of the diffraction line. Thin films have a surface thickness of roughly 1000 and may be examined using XRD [3]. Reflection high energy electron diffraction (RHEED) can be used to characterize thicker films. The presence of multiple crystallographic phases in the film can be revealed by analyzing the diffraction patterns acquired by these techniques and comparing them to standard ASTM data. The film's crystallographic phases, their relative abundance, lattice characteristics, and probable favored orientations.

The set of network planes (h k l) is identified from the standard data using the 'd' values, and the network parameters are generated using the relationships. The relationships are used to derive the lattice parameters. The lattice parameters of a crystal structure can be calculated using the relationship,

$$\frac{1}{d^2} = \frac{1}{sin^2\beta}\left(\frac{h^2}{a^2} + \frac{k^2 sin^2\beta}{b^2} + \frac{l^2}{c^2} - \frac{2hlcos\beta}{ac}\right) \tag{III.2}$$

where (h, k) and (l) are the crystal plane indices, (d) is the interplanar spacing, and (β) is the full-width half maximum. The effective crystal domain is measured by the crystalline size (D). It adds to peak broadening, and as crystalline size declines, so does the entire width. The

average D of the film is calculated using the Debye Scherrer formula [4],

$$D = \frac{k\lambda}{\beta cos\theta} \tag{III.3}$$

Where (k) is a constant known as the shape factor and is assumed to be 0.94, and (λ) is the wavelength of X-rays. The relationship, [5], is used to calculate the origin of micro strain (ε).

$$\varepsilon = \frac{\beta cos\theta}{4} \tag{III.4}$$

The dislocation density (δ) is the number of dislocation lines per unit area of the crystal and may be calculated from the crystalline size 'D' using the formula[6],

$$\delta = \frac{1}{D^2} \tag{III.5}$$

III.2 The Morphology of the Surface

Surface morphology is a subset of analytical imaging, which is a high-resolution imaging technique that uses powerful microscopes to obtain pictures of materials, objects, and products that are not visible to the human eye. These pictures are created by the exposed surface of the sample or product.

III.2.1 Electron microscope

The electron microscope is a type of microscope that creates images of samples using an electron beam. It has substantially better magnification and resolution power than an optical microscope. It is substantially bigger than an optical microscope and can view many tiny things in much greater detail. More specifics. Figure 3.2 depicts the fundamental processes for all electron microscopes. Microscopes with electrons Electron microscopes employ the signals produced by an electron beam's interaction with a sample to determine the structure, morphology, and size of the sample. Electron microscopes analyses the signals produced by the interaction of an electron beam with a sample to determine its structure, morphology, and composition.
A beam of electrons A beam of electrons is sent across the sample, and the picture is magnified using a series of lenses. The illustration. III.2 The picture is the result of electron scattering by the atoms in the sample. A A heavy atom is more effective in scattering than a low atomic number atom, therefore the presence of heavy atoms43 improves the image's contrast. All types of electron microscopes adhere to the protocols outlined above.

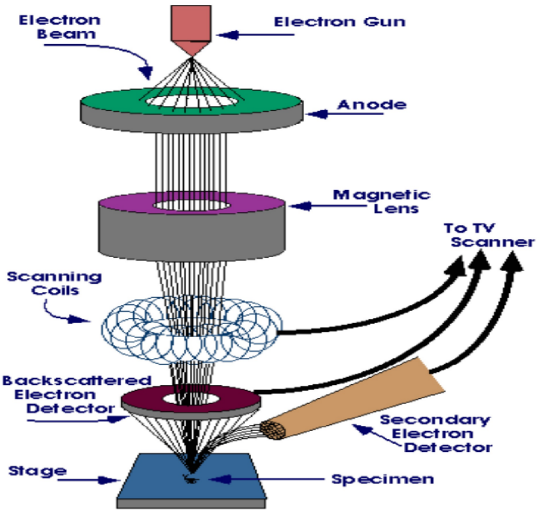

Figure III.2: An electron microscope schematic diagram.

III.2.2 Scanning electron microscopy with field emission

At magnifications ranging from 10x to 300,000x and with a nearly infinite depth of field, field emission scanning electron microscopy (FESEM) delivers topographical and elemental information. FESEM generates crisper, less electrostatically distorted pictures with spatial resolution down to a few nanometers - three to six times better than conventional SEM. Electrons are freed from a field emission source and accelerated in a high electrical field gradient in (FESEM).

As a result, each area on the item emits secondary electrons. The angle and velocity of these secondary electrons are related to the object's surface structure. The secondary electrons are captured by a detector, which generates an electrical signal. This signal is amplified and converted into a video scan-picture that may be viewed on a display or a digital image that can be stored and further processed. A JEOL JSM-7600F FESEM is shown in Figure III.3 This FESEM is utilized in this study.

Figure III.3: Setup of a field emission scanning electron microscope.

III.3 Analysis of Elements

Elemental analysis is the technique of determining the elemental and occasionally isotopic composition of a material. Elemental analysis can be either qualitative (determining which elements are present) or quantitative (determining how much of each element is present). Energy dispersive X-ray spectroscopy (EDS, EDX, or XEDS), also known as energy dispersive X-ray analysis (EDXA) or energy dispersive X-ray microanalysis (EDXMA), is an analytical method used to determine the elemental composition of a material.

III.3.1 X-ray energy dispersive spectroscopy

EDX is a chemical microanalysis technology that is used in tandem with FESEM. EDX can perform elemental analysis on regions as tiny as a nanometer in diameter, and it may be used to identify the elemental composition of individual spots or to map out the lateral distribution of elements from the imaged area. Secondary and back scattered electrons are released from the sample surface when an incoming electron beam strikes atoms.

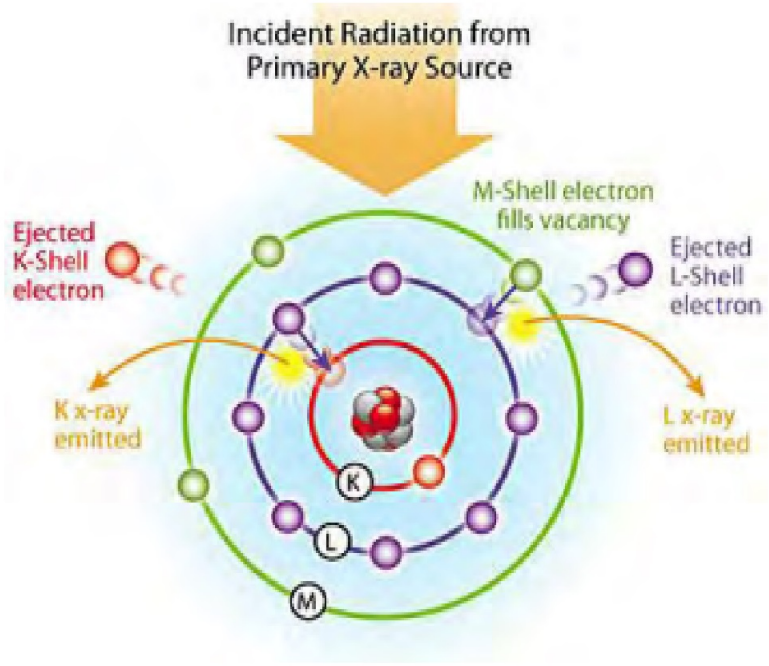

Figure III.4: Schematic of X-ray excitations in EDX analysis.

incoming beam bounces through the sample, it leaves millions of sample atoms with holes in their electron shells where the secondary electrons were. If these "holes" occur in the inner shells, the atoms are not stable. To stabilize the atoms, electrons from the outer shells will drop into the inner shells; but, because the outer shells have a higher energy state, the atom must lose some energy in order to do so. This is accomplished by the use of X-rays.

The intensity and wavelength of the X-rays released by the sample atoms are typical of not only the element of the parent atom, but also which shells lost electrons and which shells replaced them, allowing the elemental composition of the sample to be determined.
An EDX spectrum not only identifies the element that correlates to each of its peaks, but it also specifies the type of X-ray to which it belongs. A K-alpha peak, for example, corresponds to the amount of energy held by X-rays released by an electron in the L-shell moving to the K-shell. The K-beta peak (Figure:III.4) corresponds to X-rays released by M-shell electrons passing through the K-shell.

III.4 Characterization Optical

Thin film optical characteristics have been explored due to their use in many optical and optoelectronics devices. UV-visible spectroscopic measurements are used to investigate the optical characteristics of thin films. Transmission, absorption, reflection, refraction, polarization, interference, and other optical phenomena are studied. From these characteristics, optical constants such as absorption coefficient (α), direct and indirect band gap, refractive index (n), extinction coefficient (k), optical conductivity (σ_{opt}), real and imaginary component of dielectric constant, and so on may be calculated.
UV-visible transmission spectra were acquired at room temperature using a dual beam UV-visible spectrophotometer (SHIMADZU UV-1601) in the wavelength range of 200-1100 nm (Figure 3.10). Transmission spectra were obtained for CuO thin films with Ts of 300 °C, 350 °C, 370 °C, and 400 °C, as well as CuO: Zn thin films with Ts of 350 °C and concentrations ranging from 1-6 at%. During the optical absorption measurement of thin films, a cleaned glass slide is employed as the reference.

III.4.1 Beer-Lambert law

The linear connection between absorbance and concentration of an absorbing species is described by the Beer-Lambert law (or Beer's law) [7]. The general Beer-Lambert law is typically expressed as follows:

$$A = abc \tag{III.6}$$

Where 'A' is the observed absorbance, 'a' is a wavelength-dependent absorptivity coefficient, b is the route length, and c is the concentration of the analyzer. When dealing with molarity

Figure III.5: A spectrophotometer that can detect UV and visible light.

concentration units, the Beer-Lambert law is expressed as:

$$A = \varepsilon bc \tag{III.7}$$

Where (ε) denotes the wavelength-dependent molar absorptivity coefficient in $(Mcm)^{-1}$ units. Typically, experimental observations are done in terms of transmittance (T), which is defined as

$$T = \frac{I}{I_0} \tag{III.8}$$

Where I represent the light intensity after passing through the sample and Io represents the original light intensity. The following is the relationship between A and T:

$$A = -logT = -log\frac{I}{I_0} \tag{III.9}$$

Data from modern absorption devices is often shown as either transmittance or absorbance. The Beer Lambert law is obtained from an approximation for a molecule's absorption coefficient by modeling the molecule with an opaque disk whose cross-sectional area, (σ), corresponds to the area of effect seen by a photon frequency(ν). The area is greatest when the frequency of the light is furthest from resonance. Using an infinitesimal sample slab: Figure III.6 depicts the light absorption process. (I_0) represents the intensity entering the sample at (z=0), '(Iz) represents the intensity entering the infinitesimal slab at z, (dI) represents the intensity absorbed in the slab, and (I) represents the intensity of light exiting the sample. The overall opaque area on the slab caused by the absorbers is thus (σNA dz.) The percentage of

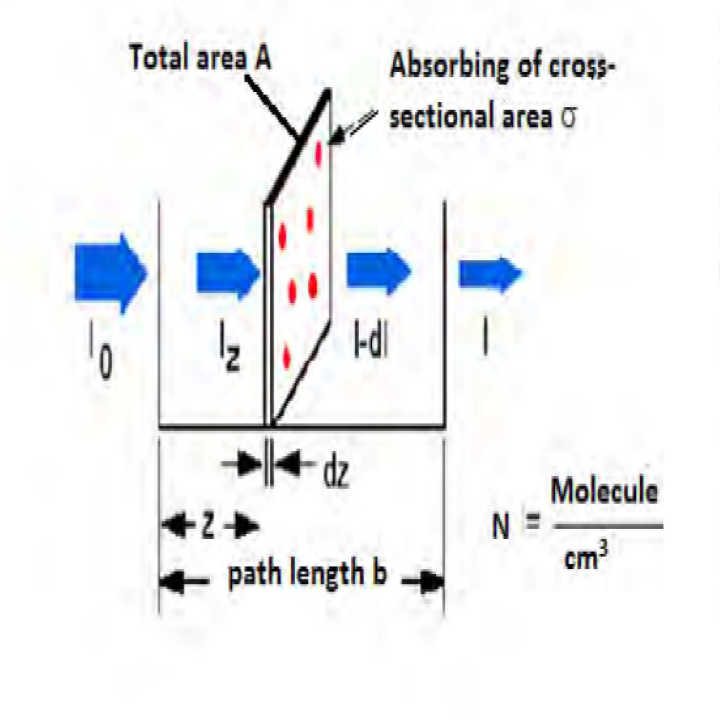

Figure III.6: Light absorption mechanism.

photons absorbed will thus be (σNA dz / A. So,)

$$\frac{dI}{Iz} = -\sigma N dz \tag{III.10}$$

Taking this equation and integrating it t=0 to z=b gives:

$$\ln (I) - \ln (Io) = -\sigma\ N\ b$$
$$\text{or } - \ln (I / Io) = -\sigma N\ b$$

Since N (molecules/cm^3) (1 mole/6.023x10^{23} mlecules) 1000 cm^3/ liter = c (moles/liter) and 2.303*log(x) = ln(x)
Then,

$$- \log(I / Io) = \sigma(6.023x10^{20} / 2.303)\ cb$$

or

$$A = \varepsilon bc = -log(I/Io) \tag{III.11}$$

Where, $\varepsilon = \sigma$ (6.023x10^{20} / 2.303) = σ(2.61x1020), and ε is called molar absorptivity. Thus, the transmitted light intensity may be represented as $I = I_0 e^{-\alpha d}$, where d is the sample path

length and is the absorption coefficient. This equation may be expressed as follows:

$$\alpha = \frac{2.303A}{d} \tag{III.12}$$

III.4.2 optical transitions: direct and indirect

The band gap, also known as an energy gap or stop band in solid-state physics and related application disciplines, is a region where a particle or quasi particle cannot propagate. The band gap in insulators and semiconductors refers to the energy difference between the top of the valence band and the bottom of the conduction band, as shown in FigureIII.7 The annihilation or absorption of photons caused by the excitation of an electron from the valence band up into the conduction band, leaving a hole in the valence band, is referred to as fundamental absorption. In such a transition, both energy and momentum must be preserved. The minimum energy in the conduction band and the highest energy in the valence band occur at distinct crystal momentum values in the case of an indirect-band gap semiconductor. Direct transitions of electrons from the valence to the conduction band require photon energy far greater than the forbidden gap. At lower energies, however, transitions can occur via a two-step process involving not just photons and electrons but also a third particle, a phonon.

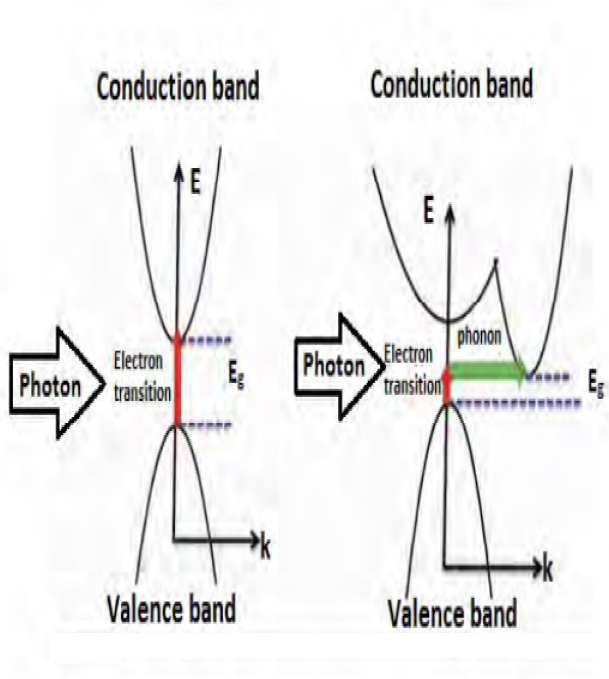

Figure III.7: Direct and indirect transitions between valence and conduction bands are depicted schematically.

A random phase model with a totally relaxed k momentum selection rate is used to evaluate

the type of absorption. N(E) has been utilized and defined as the integrated density of states.

$$N(E) = \int_{-\infty} g(E)dE \tag{III.13}$$

One such representation of the density of states per unit energy interval is

$$g(E) = \frac{1}{v}\sum \delta(E - E_n) \tag{III.14}$$

E n is the energy of the nth state, (V) is the volume, (E) is the energy at which (g(E)) is to be assessed, and (V) is the energy.

If $g_v \propto E^p$ and $g_c \propto (E - E_{opt})$, where energies are determined from the mobility edge of the valence band in the conduction band (mobility gap), and these values are substituted into an expression for the random phase approximation, the relationship obtained is $v^2 I_2 \propto (h\nu - E_0)^{p+q+1}$, where $I_2(\nu)$ is the imaginary part of the e complex permittivity. The absorption becomes photon energy dependent if both band edges' densities of state are parabolic.

$$\alpha h\nu \propto \nu^2 I_2(\nu) \propto (h\nu - E_{opt})^2 \tag{III.15}$$

Consequently, the (Tauc) relation, a generic equation that has been reduced for higher photon energies, is

$$\alpha h\nu = B(h\nu - E_{opt})^n \tag{III.16}$$

where $(h\nu)$ is the energy of the light that is absorbed, (n) is the parameter that affects how the density of states is distributed, (B) is a constant or (Tauc) parameter, and here (n = 1/2) for direct transitions and (n = 2) for indirect transitions [8]. The preceding equation may be expressed as

$$\frac{d[ln(\alpha h\nu)]}{d[h\nu]} = \frac{n}{h\nu - E_{opt}} \tag{III.17}$$

The kind of transition may be determined while determining (n) by looking at the absorption spectrum. It is possible to see a discontinuity in the $(d[ln(\alpha h\nu)]\text{versus}(h\nu)$plot at the band gap energy $(E_{opt} or E_g)$, or when i.e. $h\nu = E_{g.}$ The band gap (E_g) is determined by the discontinuity at a certain energy value. This makes it possible to calculate the direct and indirect energy gaps of thin film materials from the straight-line plots of $(\alpha h\nu)^2$ vs $h\nu$ and $(\alpha h\nu)^{1/2}$ versus $(h\nu)$.

III.4.3 Coefficient of absorption

When light shines on a semiconductor, a portion of the photons hit the surface, some of which are reflected, and the remaining photons enter the semiconductor. Some of these are transferred into the semiconductor, while the rest are absorbed by it. The excitation of electrons and photons results in the absorption of radiation by any material. Taking into account the various forms of absorption that semiconductors bring about is beneficial.

I. Switching between different energy bands in electronics.
II. Transitions in the energy band of electronics.
III. Electronic transitions of impurity atoms to regional states.
IV. Lattice vibrations
V. Atomic impurities vibrating.

In the basic absorption zone, the transmission T is given by

$$T = Aexp(-\frac{4\pi kt}{\lambda}) \tag{III.18}$$

Where "k" stands for the extinction coefficient, "t" for thickness, and "A" is constant. The principal change of T for $k^2 \ll n^2$ occurs in the pre-exponential term "A" and in the exponential term. Therefore

$$T \approx exp(-\alpha t) \tag{III.19}$$

Where $\alpha = \frac{4\pi k}{\lambda}$ is the film's absorption coefficient. Consequently, the relationship allows for the calculation of the absorption coefficient's value.

$$\alpha = -\frac{ln(T)}{t} \tag{III.20}$$

III.4.4 Extinction coefficient and refractive index

The refractive index of a material (n) is a measurement of the speed of light in that material. The ratio of the speed of light in a vacuum to the speed of light through the medium is defined as the refractive index The refractive index is calculated as follows:

n = speed of light through vacuum / speed of light through medium

n = c / v

During materials in which an electromagnetic wave is likely to lose its energy as it propagates, (n) becomes complex. The real section is usually (n) and the imaginary part is called Extinction coefficient (K). In this part, (n) and (K) will be presented in detail along with Some distracting

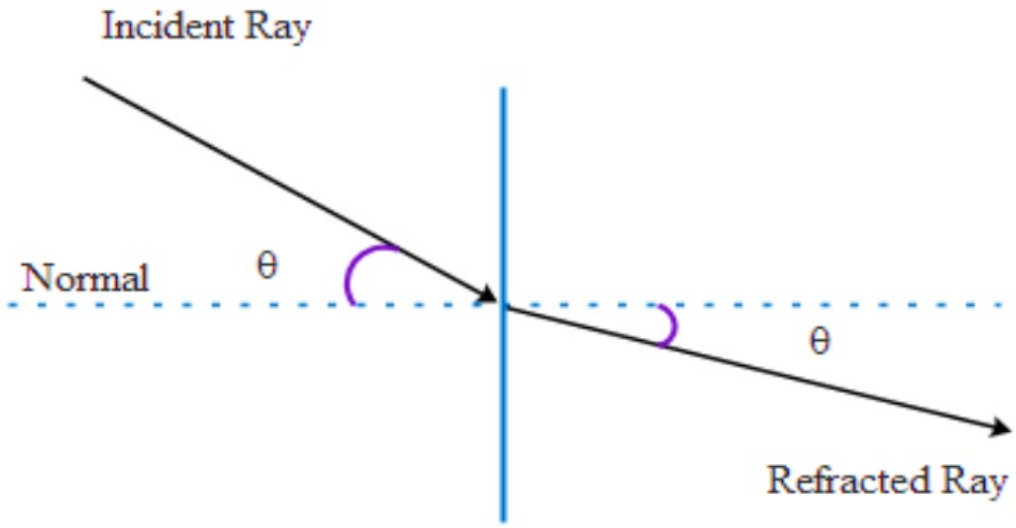

Figure III.8: Refraction of light between two different media Signs of refraction.

relationships. Employing Maxwell's equations, we obtain the well-known Maxwell's formula for (n) of matter as $(n = \sqrt{\varepsilon\mu_r})$ where (ε) is a constant insulator The constant or relative permittivity and (μ_r) is the relative permeability. If $(\mu_r = 1)$ for non-magnetizable materials, we can find, $(n = \sqrt{\varepsilon})$, and this is very useful for dielectric coupling The optical properties of the material at any specified frequency are of interest.(n)and (ε) depend on the wavelength of light, and this dependence we call scattering. In addition to scattering, electromagnetic propagation by a medium is subjected to attenuation, that is, it loses its energy, due to various loss mechanisms such as phonon generation (lattice waves), image generation, and also free carrier absorption, as well as scattering, and others. In such materials, the refractive index may become a complex function of the frequency of the light wave. The complex refractive index, denoted by the symbol (n^*), as well as the real part (n), as well the imaginary part (k), called the extinction coefficient, is considered to be related to (ε) by:

$$n^* = n - jk = \sqrt{\varepsilon} = \sqrt{\varepsilon_r - j\varepsilon_i} \tag{III.21}$$

Where$(\varepsilon_r)$and (ε_i) are, respectively, the real and imaginary parts of (ε). EquationsIII.21

$$\begin{aligned} n^2 - k^2 &= \varepsilon_r \\ and & \\ 2nk &= \varepsilon_i \end{aligned} \tag{III.22}$$

It can be obtained, (n) and (K) as follows :

$$n = (\frac{1}{\sqrt{2}})[(\varepsilon_r^2 - \varepsilon_i^2) + \varepsilon_r]^{1/2} \tag{III.23}$$

$$k = (\frac{1}{\sqrt{2}})[(\varepsilon_r^2 - \varepsilon_i^2) - \varepsilon_r]^{1/2} \tag{III.24}$$

We can determine the optical constants (n) and (k) by measuring the reflection from the surface of the material used in the experiment as a function of polarization and angle of incidence. Electromagnetic rays for normal incidence, and we obtain the reflection coefficient, (r), as follows.

$$r = \frac{(1-n^*)}{(1+n^*)} = \frac{(1-n+jk)}{(1+n-jk)} \tag{III.25}$$

The reflection (R) is determined by

$$R = |r|^2 = \left|\frac{1-n+jk}{1+n-jk}\right|^2 \qquad = \frac{(1-n)^2+k^2}{(1+n)^2+k^2} \tag{III.26}$$

There is another way to determine the value of the refractive index using the following equation

$$n = \frac{1+R}{1-R} + \sqrt{\frac{4R}{(1-R)^2} - K^2} \tag{III.27}$$

From the above, we find that when (k) is large, as an example of a range of wavelengths, we find that the absorption is strong, and the reflection is almost the same. After that, the light is reflected, and we find that any light in the medium is very weak. On the other hand, we can find the extinction coefficient by the following relation as follows

$$K = \frac{\alpha\lambda}{4\pi} \tag{III.28}$$

The optical conductivity of thin films can also be calculated This is done by the following equation

$$\sigma_{opt} = \frac{\alpha nc}{4\pi} \tag{III.29}$$

III.5 Method of measuring the thickness of the thin layer

The thickness of the film is defined as the vertical distance from any point on the surface to the other end of the film. It has a very important role in the properties of thin films and

is also considered one of the most important parameters of the film. For this, the thickness must be measured very, very carefully to obtain an accurate value. There are several methods for measuring the thickness of thin films, for example, weighing, X-ray fluorescence, there is also a pen profile technique and also a Multibeam interferometry technique [9]. Multibeam interferometry technology is used to measure the thickness of thin films. This method is based on placing two reflective surfaces close together to produce an overlap margin. It is an advanced and standard method [10]. When two reflective surfaces are placed close to each other, this produces an interference margin, this makes its measurement possible and the film thickness and surface topography can be directly determined with high accuracy. During this method, we use two types of edges to determine the thickness. The first produces edges of equal thickness, when using a monochromatic light source. The second uses a light source and produces margins of equal color order. The second method prepares for thin films. Using the Fizeau fringes method during the measurement of film thickness. For the experimental setup, there must be a low-power microscope, a monochromatic light source, a glass plate, and an interferometer. To make the edges of a Fizeau of equal thickness visible during a multibeam Interferometer consisting mainly of a thin absorbent film that is on a glass layer, and generally, an additional reflective coating is required on the surface of the film. In the event that the experimental sample is transparent and has a very smooth surface, we do not use additional paint. The film whose thickness measurement is to be determined is required to form a step on a glass substrate, and we place on top of it another flat glass plate. This is illuminated by a monochromatic parallel beam of light, during this a fringe system is produced and also viewed by a microscope that is low-power. We determine the measurement of the marginal spacing and the marginal offset (step height) by the step and use it to determine the thickness of the film. The thickness of the film "d" can then be determined by the relation.

$$d = \frac{\lambda}{2} \times \frac{b}{a} \tag{III.30}$$

Where, λ = wavelength, b = step height and a = fringe spacing. Generally, sodium light is used, where λ5893 Å. In FigureIII.9, the diagram shows how to measure the thickness using a multibeam Interferometer.

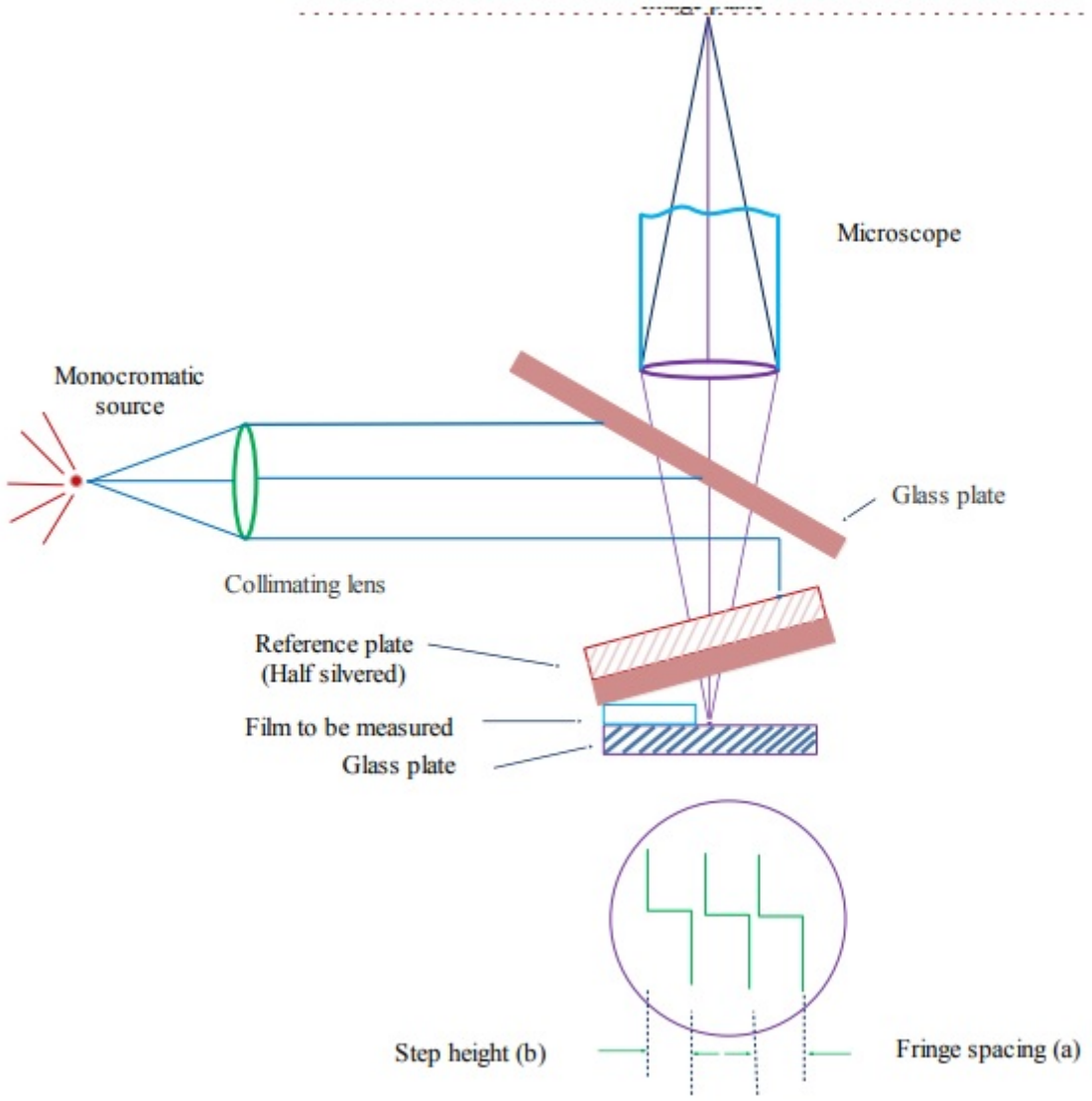

Figure III.9: Interferometer scheme for obtaining reflection of Fizeau margins of equal thickness.

References

[1] S. J. Kang, Y. H. Joung, H. H. Shin, and Y. S. Yoon, "Effect of substrate temperature on structural, optical and electrical properties of zno thin films deposited by pulsed laser deposition," *Journal of Materials Science: Materials in Electronics*, vol. 19, pp. 1073–1078, 2008.

[2] Y. Raviprakash, K. V. Bangera, and G. Shivakumar, "Preparation and characterization of cdxzn1- xs thin films by spray pyrolysis technique for photovoltaic applications," *Solar energy*, vol. 83, no. 9, pp. 1645–1651, 2009.

[3] B. Gupta and O. Agnihotri, "Structural investigations of spray-deposited cds films doped with cu, in and ga," *Philosophical Magazine B*, vol. 37, no. 5, pp. 631–633, 1978.

[4] B. E. Warren, *X-ray Diffraction*. Courier Corporation, 1990.

[5] Y. Zhao and J. Zhang, "Microstrain and grain-size analysis from diffraction peak width and graphical derivation of high-pressure thermomechanics," *Journal of applied Crystallography*, vol. 41, no. 6, pp. 1095–1108, 2008.

[6] F. Szekely, I. Groma, and J. Lendvai, "Characterization of self-similar dislocation structures by x-ray diffraction," *Materials Science and Engineering: A*, vol. 324, no. 1-2, pp. 179–182, 2002.

[7] D. F. Swinehart, "The beer-lambert law," *Journal of chemical education*, vol. 39, no. 7, p. 333, 1962.

[8] E. Davis and N. Mott, "Conduction in non-crystalline systems v. conductivity, optical absorption and photoconductivity in amorphous semiconductors," *Philosophical magazine*, vol. 22, no. 179, pp. 0903–0922, 1970.

[9] G. Siddall, "Handbook of thin film technology edited by leon i. maissel and reinhard glang. published by mcgraw-hill, maidenhead, berks, uk, and new york, ny, 1970; ca. 1200 pages. price£ 14.15.," *Thin Solid Films*, vol. 8, no. 6, p. 473, 1971.

[10] J. Israelachvili, "Thin film studies using multiple-beam interferometry," *Journal of Colloid and Interface Science*, vol. 44, no. 2, pp. 259–272, 1973.

Chapter IV

SYNTHESIS OF INDIUM DOPED COPPER OXIDE THIN FILMS

Summary

IV.1 Introduction

We can give the thin film a concept as a two-dimensional quasi-material that is created by condensation, Atomic / molecular / Ionic types of matter The preparation of a thin film goes through several sequential stages. The method of spray is considered It is the most widely used method adopted for the synthesis of a thin layer of Transparent, conductive oxide, chalcogenides, etc. compounds [1]. In this chapter Details about precursors and doping substances, the design and construction of various experimental devices and the preparation CuO:In of thin films on a glass substrate by spray are briefly discussed

IV.2 Precursor Material

Of synthesis (CuO:In) thin filmsCopper(II) sulfate, pentahedra $CuSO_4 \cdot nH_2O$ is used as a precursor material.$CuSO_4$ is non-toxic and non-flammable. It is collected from the local market. It's some typical properties are discussed below:

Property name	The amount
Chemical Name	Copper(II) sulfate
Molar Mass	249.685 $g\,mol^{-1}$.
Appearance	blue (pentahydrate)
Density	2.286 $g\,cm^{-3}$
Melting Point	110 °C
Boiling Point	650 °C
Crystal Structure	Monoclinic

Table IV.1: Properties of copper oxide

Figure IV.1: Copper oxide powder

IV.3 Doping Material

To prepare CuO:In thin films, Indium(III) chloride$InCl_3$ is used as doping material. It is and is sigma ALDRICH Product Number: 203440 collected from the local market. Some typical properties of $InCl_3$ are discussed below:

Property name	The amount
Chemical Name	Indium(III) chloride $InCl_3$
Physical state	powder
Color	white, yellow
Odor	odorless
Molar Mass	221,18 $g\,mol^{-1}$.
Density	3,46 $g\,cm^{-3}$

Table IV.2: Properties Indium(III) chloride

Figure IV.2: Indium(III) chloride

IV.4 Experimental Details

IV.4.1 Fabrication of masks

A correctly formed hole is usually required for direct deposition of a thin-film pattern. It is known as the mask. For the purpose of various experimental studies, a film of a certain size and shape is required. The visor is made of stainless steel sheets with the desired pattern parts in it. The hole was made on a lathe. The mask is placed close to the substrate to allow

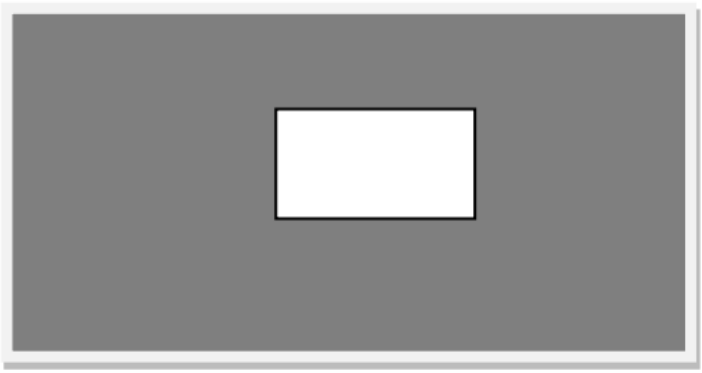

Figure IV.3: Mask for the sample.

condensation of the evaporator only in exposed areas of the substrate. The mask was prepared as in the Figure IV.3. Where the edge of the mask is smooth, so it is useful to determine the exact thickness of the film.

IV.4.2 Air compressor

Air compressor is an energy conversion machine, From Energy electric to kinetic energy by compression and air compressing. It is an electric tank type. The air compressor. A pressure gauge is installed at the outlet of the tank, which records the air pressure at the moment when air is supplied from the tank. There is a bypass control, the valve can keep the outlet pressure constant.

IV.4.3 The design of the reactor

The structure of the reactor is shown in Figure IV.4. It is a vertical batch reactor. It consists of a heater and a heat receiver. We find a hole on the side of the reactor and in the upper part for the rapid expulsion of gases during sedimentation. It helps to concentrate while the spray falls on the substrate and also provides an opening for exhaust gases at the top.

IV.4.4 Heater

The heater is an ordinary heater with a cable with a power of 1.5 kW. The top of the slab is covered with an asbestos sheet, with a small open space in the middle where the mica sheet meets. A thick stainless steel plate is placed on top of this Mica plate, figureIV.4. The substrate is placed on this receptor to obtain a uniform temperature throughout the surface of the substrate. The voltage variable controls the heater power.

IV.4.5 The fume chamber

It is a large storage room with a pitched roof and a fireplace. An exhaust fan with a regulated power supply is installed above the chimney to remove unused gases from the room. The upper and sloping side walls are made of glass aluminum. In the front part of the doors are closed. The room has disinfection options. The entire spraying system and Reactor are stored in the combustion chamber at the time of film deposition for safety and to check for air flow disturbance at the deposition site. These two points that have just been mentioned are of great importance for the spraying process in the case of outdoor decomposition.

IV.4.6 Spray head / nozzle

A single spray nozzle consists of two lattice tubes (stainless steel) mounted perpendicular to the other tube, as shown in Figure IV.4. Compressed air is quickly passed through the upper tube transversely to the mouth of the lower tube, where the other end is immersed in the spray liquid. Due to this negative pressure, the liquid rises through the tube and is expelled by compressed air in the form of fine particles (aerosols). A thin spray head produces finer spray particles. A very fine capillary tube in the form of a needle is used for the spray nozzle. The exact spray flow through the nozzle depends on the caliber of the nozzle and can vary from nozzle to nozzle.

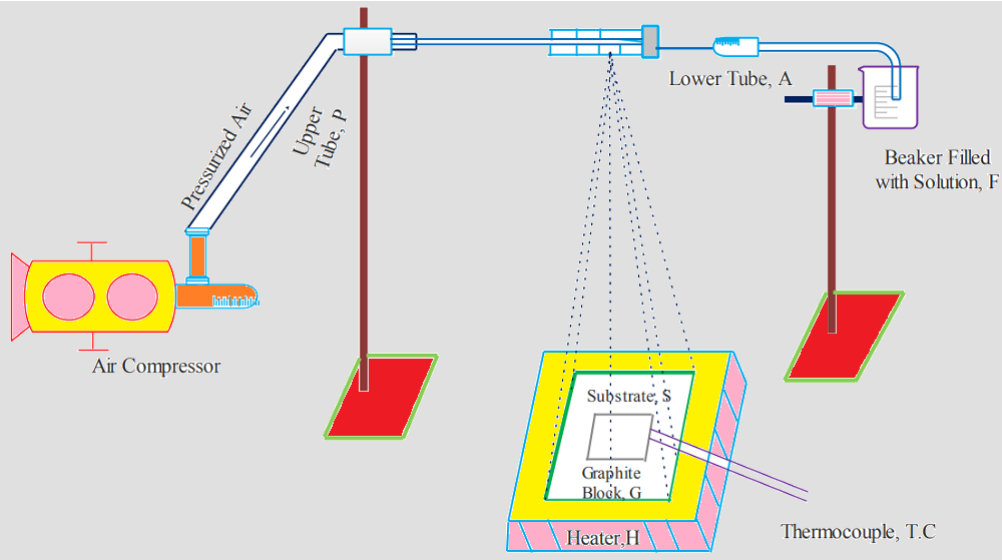

Figure IV.4: A schematic diagram of the experimental set up of the spray pyrolysis technique.

IV.5 Choice of substrate

Thin film deposition is done on solid substrates including glass, quartz, ceramics, alloys, mica, minerals, metals, semiconductors, insulators, organic materials like cellulose, plastic, polymer, rubber, and so on. The chosen substrate must be level and smooth. As well As good adherence to the deposited film [2]. There must be no chemical interaction with the deposited coating. In this investigation, non-conducting and amorphous microscope glass slides measuring 5 cm long, 2 cm broad, and 0.1 cm thick were employed as substrates.

IV.6 Substrate cleaning

The cleanliness of the substrate has a significant impact on the characteristics of the thin film put on it. Surface contamination appears as pinholes, which might result in an open resistor or localized high resistance. The following processes are used to clean the substrate: the total contamination of each substrate is first eliminated. They are washed with distilled water after being cleaned with a lukewarm aqueous solution of sodium carbonate. After washing in distilled water, the substrates are then immersed in acid diluted with water and then the glass substrate is placed in warm acetone for 10 min. Then they are washed and rinsed thoroughly with deionized water for several times. Finally, they are dried in hot air and saved for use. In the course of the whole process, the substrates are always fixed by sliding fixing forceps [3].

IV.7 Preparation of solution

The working solution is prepared by taking $CuSO_4 \cdot {}_5H_2O$ as source material. The most commonly used solvents are distilled water and ethanol. Since $CuSO_4 \cdot {}_5H_2O$ dissolves in water at room temperature, water is taken as the solvent. Since the spray system used in the present experiment operates through a partial vacuum path as the spray nozzle, the concentration of the solution prepared by the solvent is done in such a way that it can at least be drawn up by the nozzle. The higher the concentration, the lower the spray rates. A typical value of a solution concentration of 0.1 M was used in this work. For the preparation of CuO:In thin films, the aqueous solution of copper sulfate: indium chloride is used as the initial solution, respectively. In the case of CuO:In thin films, the atomic percentage of indium in solution varies in different proportions 2%-4%-6%

IV.8 Thin film deposition parameters

The characteristics of thin films produced using the SP method are affected by a number of deposition procedure parameters. Deposition parameters such as substrate temperature (T_s), spray rate (S_r), solution nature and concentration (C), deposition time (t_d), substrate material quality, atomized particle size, substrate-to-spray outlet distance (d_s), carrier air pressure, and others have an effect on film properties. The impact of various critical spray parameters is addressed here.

1) **Substrate temperature**
   The temperature of the substrate has a significant impact on the characteristics of the produced films. Higher substrate temperatures often result in the production of better crystalline films [4]. Initial nucleation density and recrystallization are the primary determinants of grain size. Changes in substrate temperature impact the composition and thickness, which in turn affects the characteristics of deposited films. The CuO:In thin films are deposited in this work at (T_s) of(380°C), which is an optimised (T_s) for (CuO)thin films.
2) **Spray rate**
   Another factor impacting the characteristics of produced films is the spray rate. Changes in spray rate have been shown to alter characteristics such as crystallinity, surface morphology, resistivity, and even thickness[5]. Lower spray rates, on average, facilitate the production of better crystalline coatings. A lower spray rate necessitates a longer deposition time to create films of the same thickness as a greater spray rate. An appropriate nozzle 'A' and altering the airflow rate can control the rate of flow of the working solution. In this study, the spray rate is practically constant at $0.08\,\mathrm{mL\,min^{-1}}$.

3) **Thickness control**

Thickness has a crucial impact on the film characteristics of thin films, unlike a bulk material [6, 7]. In the current SPT, the deposition time is the key thickness regulating factor, assuming the other parameters stay constant. Since the deposition is carried out in normal atmosphere, a direct and in situ control of thickness is not so straightforward. To manage the film thickness, hence calibration chart may be utilized. The charts are typically plots of deposition time vs thickness, and may be created at different constant substrates temperatures prior to the creation of individual experimental samples utilizing the varied solution and deposition variables. Since the rate of deposition in the current set up is quite minimal, the thickness control is thus not problematic.

4) **Sample deposition**

It has been studied before that SPT is a cost-effective process for creating CuO:In thin films [8] which consist mainly of spraying solution over a heated glass substrate. The apparatus needed to carry out the chemical spray procedure comprises a device to atomize the spray solution and a substrate heater. FigureIV.4 depicts a schematic representation of the SPT unit, and Figure IV.5 displays the experimental setup for SPT employed in this work. A large volume of (approximately 100 mL) solution is taken in the container (F) fitted with the spray nozzle (A). The clean glass substrate is placed on the susceptor of the heater (H) with an appropriate mask. The distance between the nozzle tip and the surface of the glass substrate is kept constant 25 cm.. Before delivering compressed air, the substrate temperature ((T_s)) should be kept slightly higher than the needed ((T_s)) since a minor drop in temperature is expected at the start of spraying. (T_s) is regulated by adjusting the power of the heater with a Variant. A copper constant a thermocouple is placed on the substrate to measure (Ts). When compressed air is fed through (P) at a constant pressure of (1 bar), a vacuum is generated at the tip of the nozzle, the solution is transferred to the reactor zone in the form of a spray, and a film is deposited on the heated substrate . The working solution is tuned so that 5 minutes of spray generates CuO:In thin films with thicknesses ranging from 144 to 190 nm. The chemical reaction that occurs on the heated substrate to create CuO:In might be as follows: regulated by adjusting the power of the heater with a Variant. A copper constant a thermocouple is placed on the substrate to measure (T_s). When compressed air is fed through (P) at a constant pressure of 1 bar. a vacuum is generated at the tip of the nozzle, the solution is transferred to the reactor zone in the form of a spray, and a film is deposited on the heated substrate [9, 10]. The working solution is tuned so that 5 min. of spray generates CuO:In thin films with thicknesses ranging from 144 nm to 190 nm.. The chemical reaction that occurs on the heated substrate to create CuO:In might be as follows:

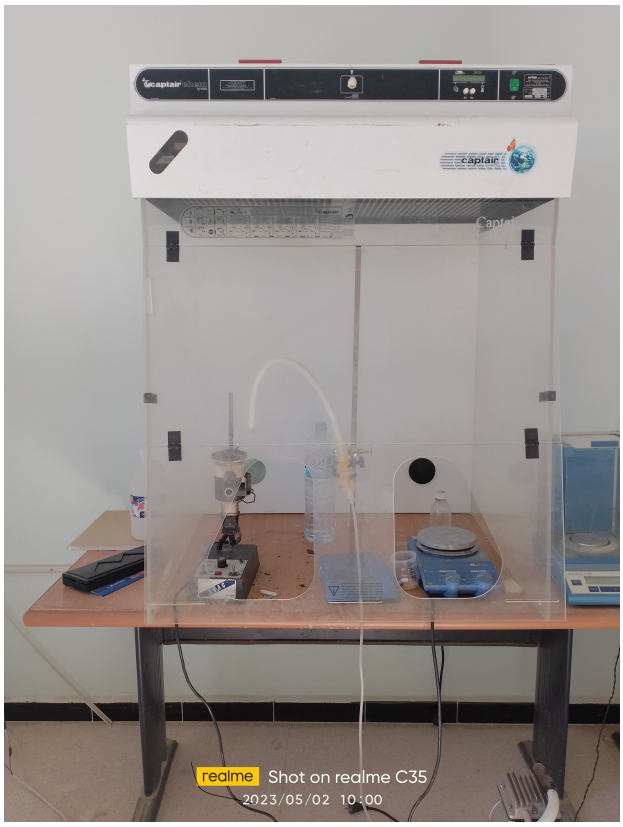

Figure IV.5: : Experimental set up of spray pyrolysis unit.

IV.9 Synthesized Sample

The table shows the synthesised samples under various settings for the research.

Sample	Solution Concentration (M)	$T_s(^0C)$	In Concentration (at%)
CuO:In	0.1	380	2,4 and 6

Table IV.3: Synthesized Sample

IV.10 Photolysis measurement

The photocatalytic decomposition of the(CuO:In) photocatalysis was quantitatively measured at room temperature under the irradiation of a UV lamp mostly emitted at 365 nm. with a power of 12 W., 230 V., and 50 Hz. It was used as a UV light source and placed parallel to the beaker as shown in IV.7[14].

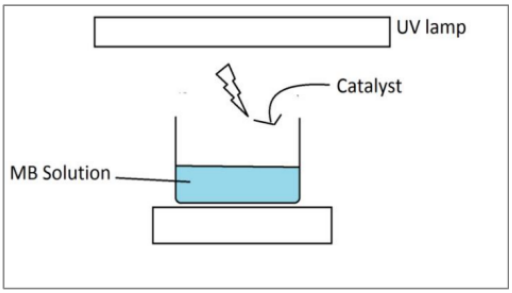

Figure IV.6: Experimental setup of photo-catalytic degradation .

Figure IV.7: UVmini-1240

The reaction was carried out with a (CuO:In) catalyst dispersed in 100mL of MB solution 5 mg/L and irradiated by UV light. MB. Approximately 4 mL of sample is withdrawn at an interval of10 min., respectively. The concentration of MB in solution was determined by measuring the absorbance at a wavelength of 664 nm using a UV-Vis spectrometer at room temperature and the results were converted to the corresponding concentration (C). The photodegradation ratio of MB was calculated using the following equation IV.1 [12, 13]

$$Photocatalyticdegradationof MB\% = \frac{c_0 - c_t}{c_0} \times 100 \tag{IV.1}$$

where C_0 is the initial concentration of MB solution and C_t is the concentration of MB solution at the time of irradiation, respectively. Moreover, the photodegradation rate constant,(k) values for the decomposition of MB dye with different amount of (CuO:In) catalyst were calculated using the first order kinetic rate reaction based on the following equation IV.2 [11, 15]

$$ln\frac{c}{c_0} = -kt \tag{IV.2}$$

References

[1] A. Antonaia, P. Menna, M. Addonizio, and M. Crocchiolo, "Transport properties of polycrystalline tin oxide films," *Solar energy materials and solar cells*, vol. 28, no. 2, pp. 167–173, 1992.

[2] L. I. Maissel and R. Glang, "Handbook of thin film technology mcgraw-hill," *New York*, pp. p12–21, 1970.

[3] C. Choudhury and H. Sehgal, "Properties of spray-deposited cobalt oxide selective coatings on aluminium and galvanised iron substrates," *Applied Energy*, vol. 10, no. 4, pp. 313–324, 1982.

[4] L. Soliman, H. Afify, and I. Battisha, "Growth impedence of pure cds films," 2004.

[5] T. Sebastian, R. Jayakrishnan, C. Sudha Kartha, and K. P Vijayakumar, "Characterization of spray pyrolysed cuins2 thin films," *The Open Surface Science Journal*, vol. 1, no. 1, 2009.

[6] L. Kadam and P. Patil, "Thickness-dependent properties of sprayed cobalt oxide thin films," *Materials chemistry and physics*, vol. 68, no. 1-3, pp. 225–232, 2001.

[7] G. Korotcenkov, V. Brinzari, and I. Boris, "(cu, fe, co, or ni)-doped tin dioxide films deposited by spray pyrolysis: doping influence on film morphology," *Journal of materials science*, vol. 43, pp. 2761–2770, 2008.

[8] R. Chamberlin and J. Skarman, "Chemical spray deposition process for inorganic films," *Journal of the Electrochemical Society*, vol. 113, no. 1, p. 86, 1966.

[9] E. Elangovan and K. Ramamurthi, "Studies on optical properties of polycrystalline sno2: Sb thin films prepared using sncl2 precursor," *Crystal Research and Technology: Journal of Experimental and Industrial Crystallography*, vol. 38, no. 9, pp. 779–784, 2003.

[10] S. Kose, E. Ketenci, V. Bilgin, F. Atay, and I. Akyuz, "Some physical properties of in doped copper oxide films produced by ultrasonic spray pyrolysis," *Current Applied Physics*, vol. 12, no. 3, pp. 890–895, 2012.

[11] Q. I. Rahman, M. Ahmad, S. K. Misra, and M. Lohani, "Effective photocatalytic degradation of rhodamine b dye by zno nanoparticles," *Materials Letters*, vol. 91, pp. 170–174, 2013.

[12] A. H. Jawad, N. S. A. Mubarak, M. A. M. Ishak, K. Ismail, and W. Nawawi, "Kinetics of photocatalytic decolourization of cationic dye using porous tio2 film," *Journal of Taibah University for Science*, vol. 10, no. 3, pp. 352–362, 2016.

[13] A. H. Jawad, A. F. Alkarkhi, and N. S. A. Mubarak, "Photocatalytic decolorization of methylene blue by an immobilized tio2 film under visible light irradiation: optimization using response surface methodology (rsm)," *Desalination and Water Treatment*, vol. 56, no. 1, pp. 161–172, 2015.

[14] H. A. Rafaie, N. F. M. Yusop, N. F. Azmi, N. S. Abdullah, and N. I. T. Ramli, "Photocatalytic degradation of methylene blue dye solution using different amount of zno as a photocatalyst," *Science Letters*, vol. 15, no. 1, pp. 1–12, 2021.

[15] N. Jain, A. Bhargava, and J. Panwar, "Enhanced photocatalytic degradation of methylene blue using biologically synthesized protein-capped zno nanoparticles," *Chemical Engineering Journal*, vol. 243, pp. 549–555, 2014.

Chapter V

RESULTS AND DISCUSSION

Summary

V.1 Introduction

The objectives of this study are the characterization of CuO:In composite thin films by SPT. Various characterizations of CuO:In thin films were performed by UV-visible spectroscopy and photocatalysis for a double blue displacement the results and the discussion about the results according to the different characteristics are shown in this chapter

V.2 Optical Properties

V.2.1 Transmittance

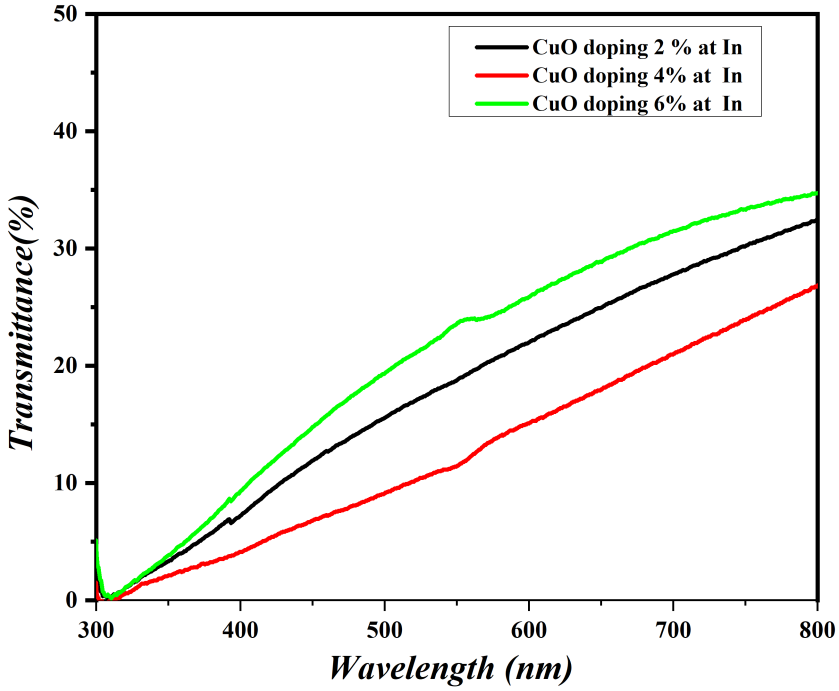

Figure V.1: Transmittance vs. wavelength graph for(2,4,6) at% CuO:In thin films deposited atTs = 380 °C.

Figure V.1 graph of optical transmittance versus wavelength for thin-film deposition of CuO:In. At concentrations from 2% to 6% at Ts = 380 °C. Figure V.1 that the value of T decreases at concentration 4% and increases at 6%, which is the largest value . T may have decreased due to a decrease in the free carrier..CuO:In.thin films are very transparent in the NIR region, with a maximum T of around 35% for a concentration of 6% In.

V.2.2 Absorbance

Figure V.2 shows a wavelength-dependent absorption curve of a thin film of doped indium copper oxide in several different doses.2 % ,4% ,6% Absorption (A) decreased with increasing indium concentration until 6 % we notice there is an increase In thin films CuO:In absorption starts at 600 nm wavelengths, this observation provides information about the direct band gap Chaudhary et al. [1] reported that the absorption starts at λ 600 nm in CuO thin films synthesized at Ts of Ts = 380 °C. From Figure V.2, it is clear that A decreases for the films with the increase in wavelength. This decrease in the absorption indicates that the presence of optical band gap in the material [2].

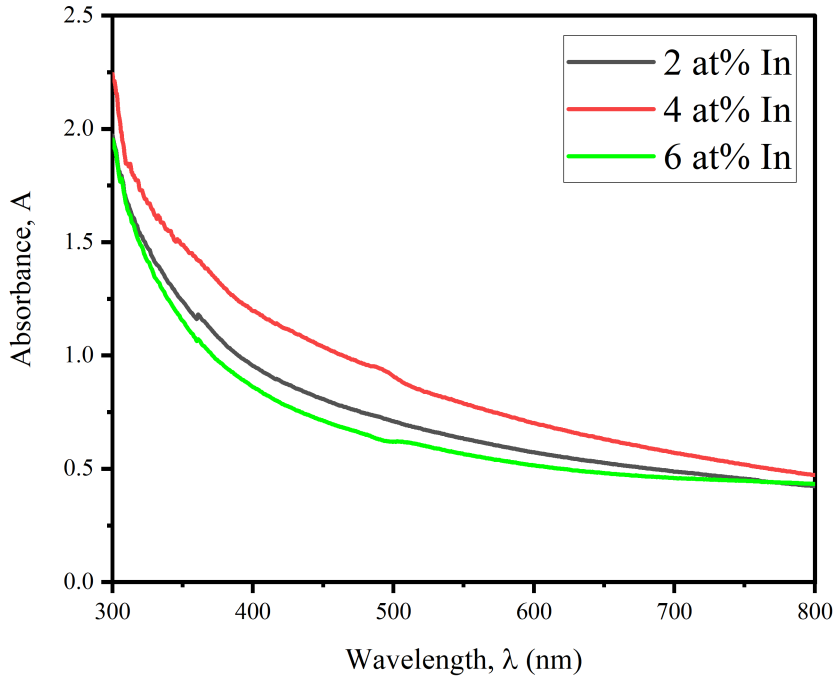

Figure V.2: Variation of absorbance with wavelength for(2,4,6) at% CuO:Inthin films deposited at Ts = 380 °C.

V.2.3 Optical band gap

The anisotropy of α with hν is analyzed by following the Tauc relation, Equation III.16, to evaluate the optical band gap of CuO:In thin films. For the optical band gap, $(\alpha h\nu)^2$ vs. hν plots of CuO:In thin films synthesized at Ts = 380 °C with 2 to 6 in % In are shown in Fig. V.3.

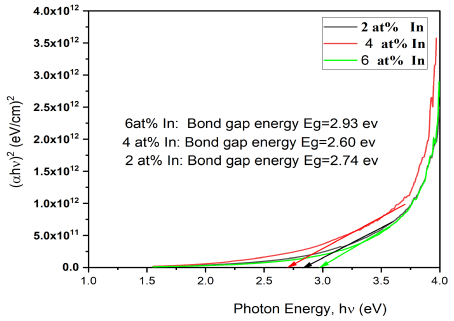

Figure V.3: Plots of $(\alpha h\nu)^2$ vs. hν for CuO:In thin films synthesized at (Ts = 380 °C) with 2 to 6 at % In concentration.

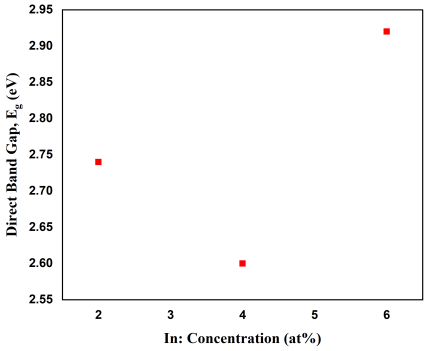

Figure V.4: Variation of direct band gap for CuO: In with In concentration (Ts = 380 °C)

Figure V.3 shows that the (E_g) value of CuO thin films with CuO: (in) thin films at concentration In varies between 2.60 eV and 2.93 eV. It is reported that the (E_g) value of CuO thin films obtained by chemical deposition ranged from 1.80 eV to 2.40 eV [4]and those prepared by RF plasma spraying were found to range from 2.10 eV and 2.55 eV [5] as an example. The example from CuO:Zn thin films deposited by PLD and SPT techniques have been reported to range from1.95 eV and 2.50 eV [6] and from 1.92 eV and 1.95 eV [7], respectively. (E_g) increases slightly with increasing doping concentration up to 4% at In and then is derived for 6 % at In. The increase in (E_g) can be attributed to the Burstein-Moss (B-M) shift [8]. The B-M effect shows that in a heavily doped semiconductor, donor electrons occupy energy levels in the lower part of the conduction band. The Pauli principle prevents energy states from being doubly occupied. Thus the valence electrons require additional energy to be excited to higher energy states in the conduction band to maintain linear momentum, and as a result (E_g) is displaced

V.2.4 Refractive Index

The refractive factor (n) was computed using the equation III.27, which was acquired from absorption measurements. Figure V.5 shows the contrast of n to the wavelength of membranes CuO:In. n is determined to be 0.069 - 1.8 of thin membranes CuO:In.

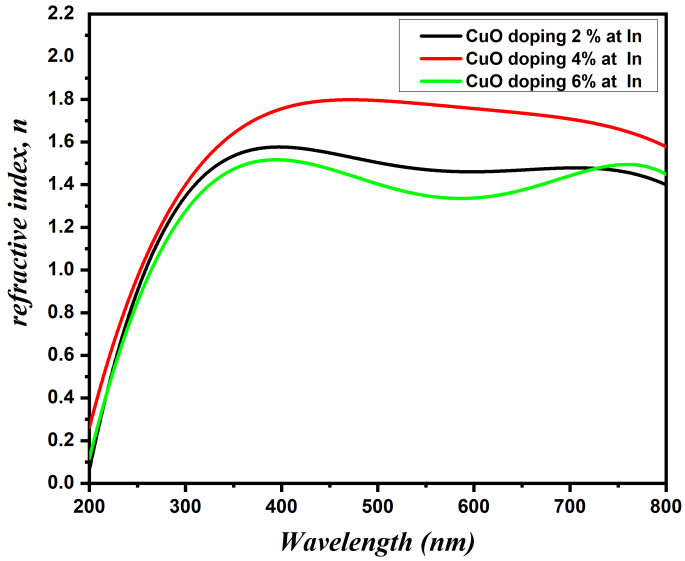

Figure V.5: Variation of refractive index for CuO:In thin films with wavelength at various In concentrations (Ts =380 °C).

Figure V.5 shows that n has the lowest In6% value in the wavelength range of 450-800 nm. When the fallen light reacts with a material with a small number of particles, the refraction is low, thereby decreasing the refraction of the film [9]. As is clearly apparent in this wavelength region, n is found above 4 at thin membranes of CuO:In,From CuO: In. Low value n inCuO:In thin film with a higher concentration than In reveals that light moves faster during these thin membranes.

V.2.5 Extinction coefficient

Extinction coefficient (k) is determined using the equation III.28 of absorption coefficient data (K) changes with the wavelength of the thin membranes deposited in figure V.6.

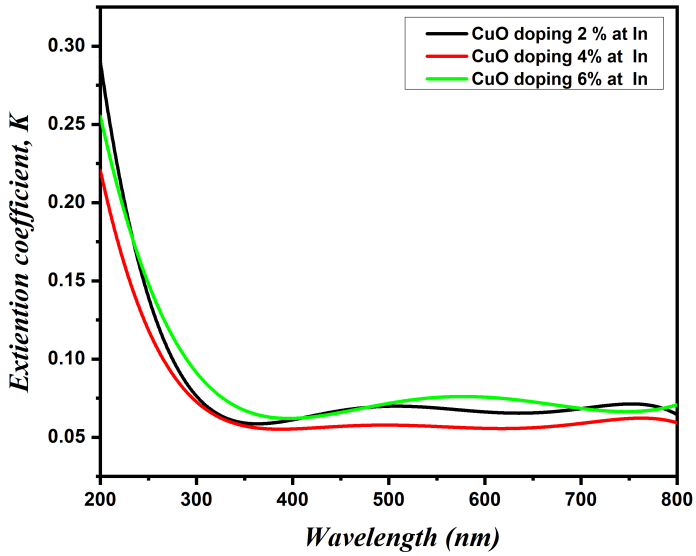

Figure V.6: Extinction coefficient varies with the wavelength of theCuO:In thin membranes at different concentrations of indium Ts = 380 °C.

Figure V.6 shows that k decreases as the wave length rises. K values vary between 0.26 and 0.05. The high value of k indicates a higher superficial roughness of the samples submitted. . The decrease of (k) can be caused by the absorption of light at the edge of the grain. This result is very close to what others have reported [10]. In Figure V.6, k decreases due to doping (In) and lower values of k are found for 4 at% CuO:In thin film up to 500 nm and above low values of k for 4 are observed at % CuO:In Thin layer of indium

V.2.6 Dielectric constants

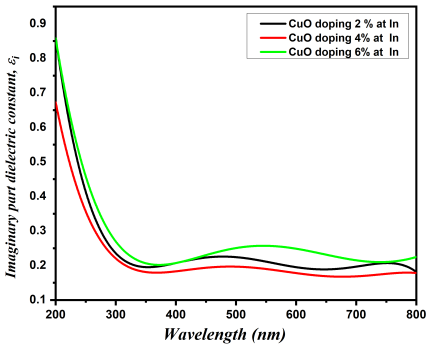

Figure V.7: Variation of imaginary part of dielectric constant with wavelength for CuO:In thin films with various In concentrations (Ts = 380 °C)

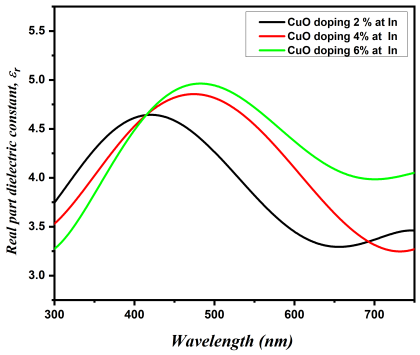

Figure V.8: Variation of real part of dielectric constant with wavelength for CuO:In thin films with various In concentrations (Ts =380 °C)

Insulation constant is a fundamental property of the substance. The real ε_r, imaginary and ε_i parts of the insulation constant are determined using the formulaIII.22. The variation of real (r) and fantasy (i) parts of the electrical insulation constant is illustrated in shape, for thin membranes CuO:In ε_r represents the magnitude of a material's polarization, it is associated with the function of slowing down the speed of light in the material. If the incoming light frequency resonates with the oscillating frequency of atoms or electrons in the medium, resonant vibrations occur and the medium absorbs light. As a result, the ε_r shows a peak value of the given frequency or wavelength. ε_r variation depends on the frequency of the incoming light. ε_r with doping decreases up to 2 at% and increases for 6 when doping% In thin CuO membranes. A similar type of insulating properties of CuO thin membranes manufactured by CBD was reported by other researchers [12].

V.2.7 Dielectric Loss

The waste of energy that goes into heating insulating material in a fluctuating electric field is known as electrical insulation loss. The buffer loss's shadow $(\tan(\delta))$ was estimated using the relationship $(\tan(\delta) = \varepsilon_i / \varepsilon_r)$. Figure V.9 depicts the response of thin indium membranes to wavelength for CuO:InThin membranes diminish In $(\tan(\delta))$ when zinc steroids increase up to 4% and subsequently to 6% concentration In. The $(\tan(\delta))$ vs. wavelength graph also revealed that $(\tan(\delta))$ values steadily drop as wavelength rises.

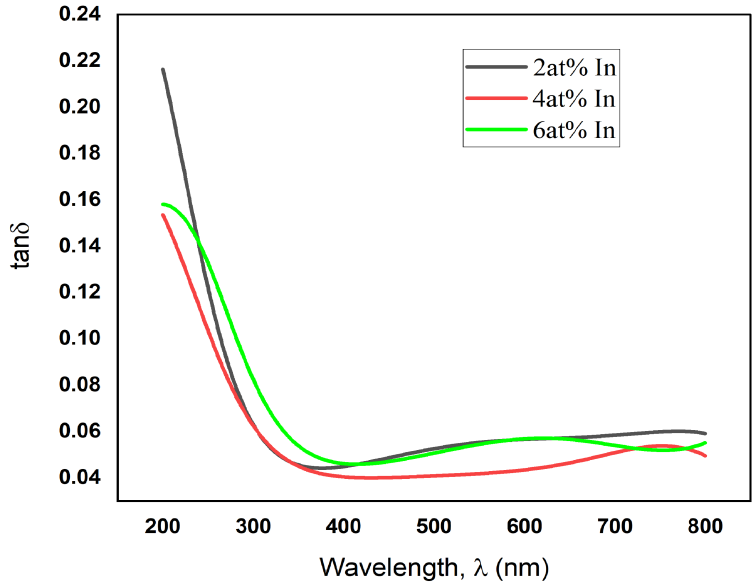

Figure V.9: Variation of dielectric loss with wavelength forCuO:Inthin films with(2,4,6) at% concentration synthesized at Ts = 380 °C.

V.3 Methylene Blue Degradation

The photodegradation kinetics of mob dye was measured in the presence of indium-doped copper oxide layers with different inoculation degrees 2-4-6% and then treated by UV-visible spectroscopy on a 200 nm to 1100 nm topology during certain time periods in addition to these three samples, we conclude in our study In a tube of methylene blue solution that was also subjected to light treatment, Figure V.10 shows the graph of the photodegradation kinetics of MB dye as a function of time, showing the obtained results

1) The photodegradation of methylene blue dye mob is at its peak after a period of time estimated at five minutes of treatment for all studied films with different indium concentrations, where it is the greatest possible at the basic absorption edge of the films that reach the highest percentage of 1, which indicates the survival of the methylene blue dye Mb It does not decompose at the beginning of the photocatalytic process

2) By comparison of the values of the photolysis of methylene blue dye, we notice that they decrease with increasing indium concentration, as their values reach approximately (0.98-0.875) at different indium concentrations 2-4-6%

3) By comparing the rates of photolysis of methylene blue dye, we notice a convergence in the ratios between the copper oxide slide in which the concentration of indium is 2% and the methylene blue container, where after a period of time of light treatment of up to 30 minutes, these percentages correspond to the value 0.98, this slight change in the percentage of dissolution of the methylene blue dye Mb, which is estimated at 0.02, indicates a lack of photocatalysis of the membrane

4) While the concentration is 4%, we obtain an average value of the absorption rate and the dissociation of the methylene blue dye, which reaches approximately 0.96.

5) While the disappearance of methylene blue dye accelerates when the slide in which the concentration of indium is 6% It is close to 0.875 as a result of the high absorbance of the membrane, and from it we find that the photo treatment time and the indium grafting concentration have a major role in the photocatalysis process

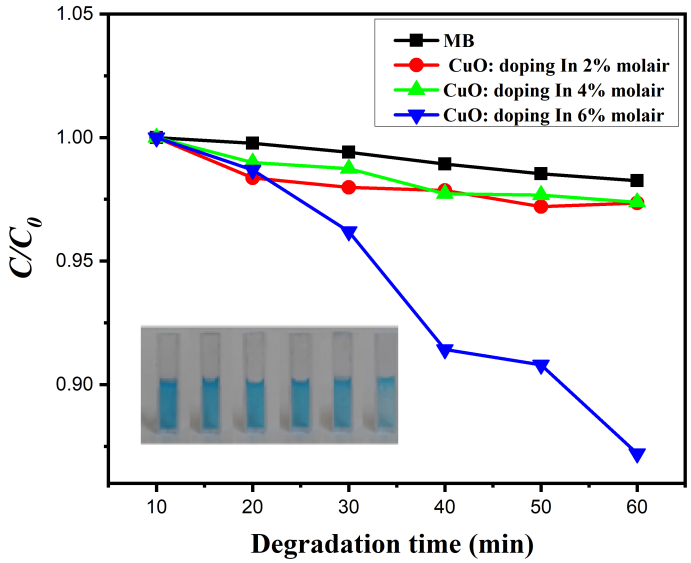

Figure V.10: Photodegradation of MB at different dye concentrations..

The photocatalysis of ultraviolet rays (uv-visbl) leads to the collision of high-energy photons, (hν), with the atoms, the thin film of indium-doped copper oxide, which results in an energy exchange with electrons that become free, and from it the transition from the valence layer to the conducting layer, leaving behind gaps or holes, and this stimulation It allows electrons to disintegrate the chemical bonds of methylene blue MB, and thus its decomposition, where we find that the higher the concentration ratio, the greater the generation of free electrons, and thus evidence of increased stimulation of the membrane deposited at a concentration of Figure 6. With the passage of ultraviolet treatment time, it completely decomposes to become methylene blue Mb with a transparent color as a result of the photocatalysis of the membranes and its high absorption, which was confirmed by previous studies

V.4 Methylene Blue Degradation Coefficients Calculation

Figure 2 shows a study of schematic diagrams of the partial decomposition kinetics under different concentrations of indium oxide to precipitate copper oxide against the irradiation time of ultraviolet radiation (UV-visible). Absorbance strength of the studied samples of copper oxide doped with indium at different concentrations (2%-4%-6%)

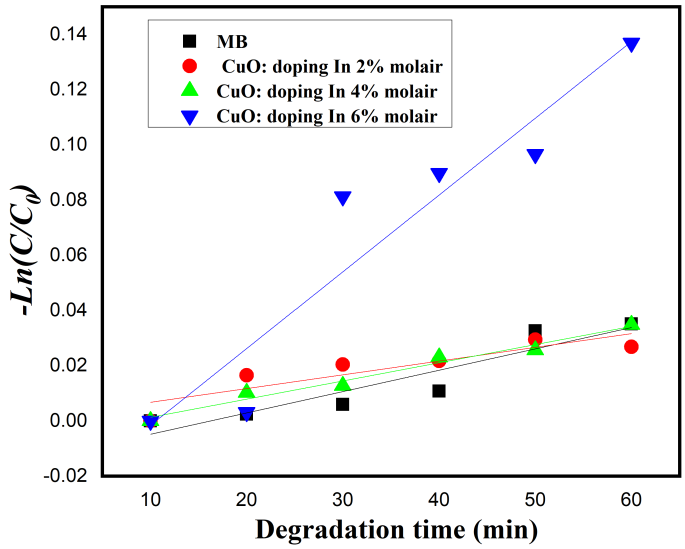

Figure V.11: The plot of ln C/C0 vs. time (at different concentrations of MB).

- Where we find the convergence between the samples at the beginning of the phototreatment, which reaches approximately (0.00-0.009), the absorbance percentage is low at the beginning, after a period of time of 5 minutes, the methylene blue solution is at the beginning of its reaction and decomposition as a result of the photocatalysis of the various samples

- Then the values of each of the copper oxide doped with indium at concentration 2, placed in a methylene blue solution, are compared to a container of methylene blue alone in parallel during photo treatment with ultraviolet rays, which increase with the passage of time to reach the value (0.029), where the speed of the absorption process in this case is weak

- While the copper oxide film with a concentration of indium 4 takes average values of the absorption rate reaching approximately (0.05).

- While the dissociation values of methylene blue for the membrane with a concentration of indium 6 accelerate, as it takes maximum values of the absorbance ratios with the passage of time to reach after half an hour a value of (0.13)

It is explained by the good coordination of the atoms of the material in which the inoculation concentration is high, in addition to that the time period of irradiation helped to increase the generation of free electrons, which indicates an increase in the absorbance of optical photons,

which in turn increases the transparency of the solution. following relationship

$$tan\beta = \frac{\Delta(-ln(\frac{c}{c_0}))}{\Delta t} \tag{V.1}$$

sampl	Rate constant $k \times 10^{-4}(min^{-1})$
MB	0.03505
In at 2%	0.02684
In at 4%	0.03477
In at 6%	0.13688

Table V.1: Dissociation rate changes of the methylene blue pigment of copper oxide layers with Indium doping at concentrations of 2%-4%-6%.

The results are recorded in the following table. Through the values recorded in the table, we note that the dissociation coefficient for methylene blue dye, it increases with increasing indium concentration in the copper oxide membranes, as well as the time of treatment with ultraviolet radiation, as its values (0.03505, 0.02684 ,0.03477, 0.13688) change corresponding to concentrations (2%-4%-6%), which confirms the increase in donor levels near the transport band, and thus an increase in the number of free electrons that absorb photons.
In general, the decomposition of a methyl bromide solution by indium-doped copper oxide particles can be explained by the mechanism below [13]. When the photocatalysis (CuO:In) is irradiated with light with an energy higher or equal to the beam gap, an electron located in the valence band (e_{cb}^{-})will be excited to the conduction band and leave a generation of a hole in the valence band (h_{vb}^{+}) on the surface of the cuo particles as shown in (Equation (4)) [14]. This excited $(E_c band h_{vb}^{+})$ can be recombined and fall into the trap of unstable surface States or interact with electron donors and adsorbed receptors on the semiconductor surface. After that, the holes can react with water adhering to the surface of theCuO:In particles to form a highly reactive hydroxyl cleft (OH) as in ((5)). At the same time, oxygen acted as an electron acceptor by forming a radical anion of superoxide (O_2^{-})as in ((6)). MB was completely hydrolyzed and removed through direct oxidation by OH radicals and (O_2^{-}) radicals as shown in ((7)).

$$\mathrm{CuO} + h\nu(\mathrm{UV}) \rightarrow \mathrm{e}_{cb}^{-} + h_{vb}^{+} \tag{V.2}$$

$$h_{vb}^{+} + \mathrm{H_2O} \rightarrow \mathrm{H^{+}} + \mathrm{OH} \tag{V.3}$$

$$\mathrm{e_{cb}}^{-} + \mathrm{O_2} \rightarrow \mathrm{O_2} \tag{V.4}$$

$$\mathrm{O_2^{-}} + \mathrm{OH} + \mathrm{dye} \rightarrow degeaded produc \tag{V.5}$$

References

[1] Y. S. Chaudhary, A. Agrawal, R. Shrivastav, V. R. Satsangi, and S. Dass, "A study on the photoelectrochemical properties of copper oxide thin films," *International Journal of Hydrogen Energy*, vol. 29, no. 2, pp. 131–134, 2004.

[2] S. Rejith and C. Krishnan, "Optical characterizations of zn-doped cuo nanoparticles," *Sci. Acta Xaver*, vol. 4, p. 91, 2013.

[3] A. S. Kumar, K. Perumal, P. Thirunavukkarasu, *et al.*, "Structural and optical properties of chemically sprayed cuo thin films," *Optoelec. Advan. Mater.–Rapid Commun*, vol. 4, no. 6, pp. 831–833, 2010.

[4] M. R. Johan, M. S. M. Suan, N. L. Hawari, and H. A. Ching, "Annealing effects on the properties of copper oxide thin films prepared by chemical deposition," *Int. J. Electrochem. Sci*, vol. 6, no. 12, pp. 6094–6104, 2011.

[5] M. Nesa, "Characterization of zinc doped copper oxide thin films synthesized by spray pyrolysis technique," 2016.

[6] H. Faiz, K. Siraj, M. Rafique, S. Naseem, and A. Anwar, "Effect of zinc induced compressive stresses on different properties of copper oxide thin films," *Indian Journal of Physics*, vol. 89, pp. 353–360, 2015.

[7] M. Engin, F. Atay, S. Kose, V. Bilgin, and I. Akyuz, "Growth and characterization of zn-incorporated copper oxide films," *Journal of electronic materials*, vol. 38, pp. 787–796, 2009.

[8] E. Burstein, "Anomalous optical absorption limit in insb," *Physical review*, vol. 93, no. 3, p. 632, 1954.

[9] S. Kose, F. Atay, V. Bilgin, and I. Akyuz, "Some physical properties of copper oxide films: The effect of substrate temperature," *Materials Chemistry and Physics*, vol. 111, no. 2-3, pp. 351–358, 2008.

[10] A. Parretta, M. Jayaraj, A. Di Nocera, S. Loreti, L. Quercia, and A. Agati, "Electrical and optical properties of copper oxide films prepared by reactive rf magnetron sputtering," *physica status solidi (a)*, vol. 155, no. 2, pp. 399–404, 1996.

[11] V. Dhanasekaran and T. Mahalingam, "Electrochemical and physical properties of electroplated cuo thin films," *Journal of Nanoscience and Nanotechnology*, vol. 13, no. 1, pp. 250–259, 2013.

[12] N. Saadaldin, M. Alsloum, and N. Hussain, "Preparing of copper oxides thin films by chemical bath deposition (cbd) for using in environmental application," *Energy procedia*, vol. 74, pp. 1459–1465, 2015.

[13] K. A. Isai and V. S. Shrivastava, "Photocatalytic degradation of methylene blue using zno and 2% fe–zno semiconductor nanomaterials synthesized by sol–gel method: a comparative study," *SN Applied Sciences*, vol. 1, pp. 1–11, 2019.

[14] W. K. Tan, K. A. Razak, Z. Lockman, G. Kawamura, H. Muto, and A. Matsuda, "Synthesis of zno nanorod–nanosheet composite via facile hydrothermal method and their photocatalytic activities under visible-light irradiation," *Journal of Solid State Chemistry*, vol. 211, pp. 146–153, 2014.

Chapter VI

CONCLUSIONS AND SUGGESTIONS FOR FUTURE WORK

Summary

CONCLUSIONS AND SUGGESTIONS FOR FUTURE WORK

VI.1 Conclusions

In this research work CuO:In thin films were deposited at a temperature of Ts = 380 °C. by SPT. The indium concentration in CuO thin films ranged from 2% to 6%. The thickness of the films is measured in the range of 144 to 190 nm. The effect of indium concentration on the optical and photocatalytic properties represented by ultraviolet spectroscopy was studied, with the effect of increasing the concentration of indium on the dissolution of methylene blue dye for CuO:In thin films. The results of the present work are summarised, and the following noteworthy conclusions are drawn From the UV Vis NIR spectral measurements it is seen that all the composite films are highly transparent in the NIR region. 7.72% The maximum T is about 87% for 4% CuO:In thin films. The direct band gap of CuO thin films increases with increasing indium concentration, up to 4% in CuO:In thin films. (n) Increases with increasing In concentration up to 4% in CuO:In thin films in the (NIR) region.(k) decreases with increasing In concentration up to 4% in CuO:In thin films. Through the optical properties investigations it can be seen that the band gap can be increased while maintaining an electrical resistivity similar to that of pure CuO.We also found that the photodegradation kinetics of methylene blue decrease between 0.98 and 0.875 at an indium concentration (2-4-6) during a time of 30 minutes as the absorbance ratio increases to a value of (0.13) at the copper oxide membrane activated by indium with a concentration of 6. We also found that these layers had good dissociation coefficients for methylene blue dye, which increased with increasing indium concentration and phototreatment time. Thus, it can be inferred from the results of this research that the films may be useful in solar cells, gas sensors, optoelectronic devices, and also in the field of photocatalysis and the purification of water and air from organic pollutants.

VI.2 Suggestions for future work

Further investigations are required to explain the different properties in detail, which will help in discovering suitable applications for CuO:In thin films. For a further understanding of this substance, the following studies can be carried out:

1) Studying the surface roughness by atomic force microscopy

2) X-ray photoelectron spectroscopy study

3) Studying the variation of the structural, optical, and electrical properties of CuO:Zn thin films with annealing temperature and deposition time

Accessories

Summary

Accessories

VI.3 Summaries

The following are summaries in the three languages English French Arabic

VI.4 code html

In addition to HTML code for calculating some optical properties
from a txt file containing values of permeability and wavelength,
the output is in the form of an Excel file

Abstract

In this work, we have studied some optoelectronic properties, dielectrics with and without taking into account the effect of the compositional disorder of ternary alloys $Zn_XCd_{1X}S$. These alloys are of great interest for the design of optoelectronic devices such as solar cells, luminescent devices and laser diodes. The method used is that of the local empirical pseudopotential (EPM) coupled with the virtual crystal approximation (VCA) which includes the effect of disorder compositional by the introduction of an effective potential of the disorder. This method is simple and gives quick and generally reliable results. The agreement between our results and the data known in the literatures, on the studied parameters, turns out reasonably good. All the studied parameters vary monotonically according to of the composition x of the Zinc Particular attention has been focused on the effect of compositional disorder on the energy gaps$E_\Gamma^\Gamma, E_\Gamma^X, E_\Gamma^l$ the refractive index, the two dielectric constants of the alloy $Zn_XCd_{1-X}S$ The latter proves to be very important and therefore we cannot neglect it.

Résumé

Dans ce travail, nous avons étudié quelques propriétés optoélectroniques, diélectriques avec et sans tenir compte de l'effet du désordre compositionnel des alliages ternaires $ZnXCd_{1X}S$. Ces alliages ont un intérêt important pour la conception des dispositifs optoélectroniques tels que, les cellules solaires, les dispositifs luminescents et les diodes laser. La méthode utilisée est celle du pseudo-potentiel empirique local (EPM) couplée avec l'approximation du cristal virtuel (VCA) qui inclut l'effet du désordre compositionnel par l'introduction d'un potentiel effectif du désordre. Cette méthode est simple et donne des résultats rapides et en général fiables. L'accord entre nos résultats et les données connues dans les littératures, sur les paramètres étudiés, s'avère raisonnablement bon. Tous les paramètres étudiés varient monotoniquement en fonction de la composition x du Zinc Une attention particulière a été accentuée sur l'effet du désordre compositionnel sur les gaps d'énergies$E_\Gamma^\Gamma, E_\Gamma^X E_\Gamma^l$ l'indice de réfraction, les constantes diélectriques de l'alliage $ZnXCd_{1X}S$ Ce dernier s'avère très important et nous ne pouvons pas le négliger. .

ملخص

في هذا العمل قمنا بدراسة الخواص الالكترونية، الضوئية ، طول الموجة و خواص العزل الكهربائي مع و بدون أخذ اعتبار لتأثير العشوائي في $ZnXCd_{1X}S$السبائك الثلاثية مقرونة بتقريب البلورة الافتراضية EPM))التركيب. في هذه الدراسة تم استعمال الطريقة التجريبية لشبه الكمون هذه السبائك لها اهمية كبيرة في تصميم الأجهزة الالكترونية الضوئية مثل : الخلايا الشمسية و (VCA). المركبات المضاءة و الديودات الليزرية. كل المقادير المحسوبة تمت دراسة تغيرها بدلالة التركيز x الزنك علي طول المجال [0-1] فى هذه الطريقة المستعملة ،الحسابات تكون بسيطة ،سريعة و اكثر دقة . التوافق بين النتائج المتحصل عليها و المعطيات المتوفرة النظرية منها و التجريبية هو عموما مقبول. يحدث انتقال علي الشكل المباشر. يجب لفت النظر في بنية عصابات الطاقة للمركب النصف ناقل العشوائي في التركيب للدراسة تغير تأثير أن إلى النظر $E_{\Gamma}^{\Gamma}, E_{\Gamma}^{X} E_{\Gamma}^{l},$ قرينة الانكسار، طول الموجة و ثوابت يجب اخذه بعين الاعتبار ولا يمكن اهماله$ZnXCd_{1X}S$العزل الكهربائي للسبيكة :Résumé

الكلمات المفتاحية :

```
<!DOCTYPE html>
<html>
<head>
  <title>Optical Properties Calculation</title>
  <script src="https://unpkg.com/xlsx/dist/xlsx.full.min.js"></script>
  <script>
    function calculateOpticalProperties() {
      var fileInput = document.getElementById('fileInput');

      var file = fileInput.files[0];
      var reader = new FileReader();

      reader.onload = function(e) {
        var contents = e.target.result;
        var lines = contents.split('\n');

        var data = [];
        data.push(["Wavelength (nm)", "Transmittance", "Reflectance",
"Absorption", "Absorption Coefficient (α)", "Wave Number (K)", "Energy (E)",
"Refractive Index (n)"]);

        for (var i = 0; i < lines.length; i++) {
          if (lines[i].trim() !== '') {
            var values = lines[i].split(',');
            var wavelength = parseFloat(values[0]);
            var transmittance = parseFloat(values[1]);

            var reflectance = 1 - transmittance;
            var absorption = Math.log10(transmittance);
            var alpha = 2.303 * absorption;
            var waveNumber = (alpha * wavelength) / (4 * Math.PI);
            var energy = 1240 / wavelength;
            var refractiveIndex = 2.998 * Math.pow(10, 8) / (wavelength *
Math.pow(10, -9));

            data.push([
              wavelength.toFixed(3),
              transmittance.toFixed(3),
              reflectance.toFixed(3),
              absorption.toFixed(3),
              alpha.toFixed(3),
              waveNumber.toFixed(3),
              energy.toFixed(3),
              refractiveIndex.toFixed(3)
            ]);
          }
        }

        var workbook = XLSX.utils.book_new();
        var worksheet = XLSX.utils.aoa_to_sheet(data);
        XLSX.utils.book_append_sheet(workbook, worksheet, "Sheet1");

        var excelBuffer = XLSX.write(workbook, { bookType: 'xlsx', type: 'array'
});
        saveExcelFile(excelBuffer, 'output.xlsx');
      };

      reader.readAsText(file);
    }

    function saveExcelFile(buffer, filename) {
      var data = new Blob([buffer], { type: 'application/octet-stream' });
      var url = URL.createObjectURL(data);
```

```
      var downloadLink = document.getElementById('downloadLink');
      downloadLink.href = url;
      downloadLink.download = filename;
      downloadLink.style.display = 'block';
    }
  </script>
</head>
<body>
  <h1>Optical Properties Calculation</h1>
  <label for="fileInput">Select Data File:</label>
  <input type="file" id="fileInput">
  <br>
  <button onclick="calculateOpticalProperties()">Calculate</button>
  <br><br>
  <h2>Download Results:</h2>
  <a id="downloadLink" style="display: none;">Download Output</a>
</body>
</html>
```